Proposal of a New Double-Nozzle Technique for In-Gas-Jet Laser Resonance Ionization Spectroscopy

Victor Varentsov *

Posted Date: 12 April 2023

doi: 10.20944/preprints202304.0251.v1

Keywords: radioactive atomic beams; gas stopping cell; supersonic gas jet; in-gas-jet laser resonance ionization spectroscopy; double-nozzle technique; gas dynamic and Monte Carlo simulations

Article

Proposal of a New Double-Nozzle Technique for In-Gas-Jet Laser Resonance Ionization Spectroscopy

Victor Varentsov *

Facility for Antiproton and Ion Research in Europe (FAIR), Planckstraße 1, 64291 Darmstadt, Germany; victor.varentsov@fair-center.eu; Tel.: +49 6159711638

Abstract: In this paper a new double-nozzle technique for in-gas-jet laser resonance ionization spectroscopy is proposed. The functionality of this new technique we explored by detailed gas dynamic and Monte Carlo atom-trajectory simulations, which results are presented and discussed. The results of similar computer simulations for JetRIS setup (as a typical representative of the conventional nowadays in-gas-jet technique) are presented and discussed as well. The direct comparison of calculation results for proposed new technique with the conventional one shows that the double-nozzle technique has many advantages compared with that one used in the JetRIS setup at GSI for future high-resolution laser spectroscopic study of heaviest elements. To fully implement the proposed new technique to all existing (or under construction) setups for in-gas-jet laser resonance ionization spectroscopy, it will be enough just replace the used their supersonic nozzle by the miniature double-nozzle device described in the paper.

Keywords: radioactive atomic beams; gas stopping cell; supersonic gas jet; in-gas-jet laser resonance ionization spectroscopy; double-nozzle technique; gas dynamic and Monte Carlo simulations

1. Introduction

For the studies of nuclear, atomic and chemical properties of radioactive elements, different techniques with the use of gas stopping cells are conventionally used. The primary energetic radioactive ions injected into a gas cell filled with the high-purity buffer gas (usually it is helium or argon) by passing through a thin entrance window. Due to a number of their collisions with buffer gas atoms, ions decelerate down to the gas flow velocity and thermalized. To speed up the transport of ions through big-sized gas cells, a DC gradient electric field is applied. In this case, the ion velocity is determined as a product of applied electric field in [volt cm^{-1}] and ion mobility coefficient in [cm^2 sec^{-1} $volt^{-1}$].

Near the extraction nozzle having the small throat diameter, ions are extracted out of the gas cell into vacuum conditions by supersonic buffer gas jet. Description of various gas cell apparatus readers can find elsewhere, for example, in [1-19] and links within them.

The extraction of the ions into high vacuum is finally performed with the use of radiofrequency quadrupoles (RFQ) [7, 8, 11 and 20–26] or radio-frequency sextupoles (SPIG) [9, 15] installed downstream for the ion beam transportation and focusing. Instead of traditional RFQ and SPIG rod-structures, a simple, compact and effective gas dynamic RF-only funnels can be used, as well. The review on the RF-only funnel technique one can find in our recent work [27].

The other way to investigate the nuclear and atomic properties of radioactive elements extracted from the gas cell is the use of laser spectroscopy techniques. One can read about, e.g. in recent reviews [28, 29] and presentation review of Piet Van Duppen [30].

The most attractive and promising nowadays method of laser spectroscopy for studying the properties of radioactive elements is the so-called method in-gas-jet laser resonance ionization spectroscopy that have been first proposed and experimentally tested in KU Leuven [31]. Briefly, it consists of the following. Under applied DC electric field gradient, the thermalized in the high purity argon ions are transported through the gas cell and focused to a tip of metallic hot filament. The tip of the filament has installed on the axis of exit flow channel in front of the nozzle. After collection of ions on the filament and subsequent their thermal evaporation as neutral atoms, they are transported

by only the carrier gas flow through the converging-diverging nozzle into the vacuum gas-jet chamber. Two lasers in cross beam geometry perform the high-resolution and efficient resonance excitation and ionization of the extracted into the gas-jet chamber neutral atomic beam. One laser beam (we will refer to as a Laser-1) directed along the axis in upstream the gas flow direction excites atoms of interest, and the second one (we will refer to as Laser-2) directed perpendicular to the gas jet ionizes these exited atoms. Then the ionized by the Laser-2 atoms transported as the ion beam by the carrier gas jet to the bended RFQ (e.g., S-shaped [31], or bend 90 degrees [32]). This curved RFQ allows for the axial laser beam injection into the gas jet and differential vacuum pumping, as well. The schematics and descriptions of various setups for the in-gas-jet laser resonance ionization spectroscopy one can find e.g. in Refs. [29–37].

The article has two following goals.

The first goal - is a detailed quantitative study of the atomic beam extraction from the gas stopping cell and then its formation and cooling in the supersonic argon gas jet under the described above traditional approach to the *in-gas-jet resonance ionization laser spectroscopy*. As a typical representative for this study, we have chosen the experimental gas-jet apparatus [32, 33] recently created for high-resolution laser spectroscopy of the heaviest elements at the Separator for Heavy Ion reaction Products (SHIP) at GSI, Darmstadt. This project called JetRIS is under development at GSI.

The second goal - is the proposal and detailed exploration of a new double-nozzle technique for its application in-gas-jet resonance ionization laser spectroscopy.

The both goals we have reached by means of computer experiments, which were consisted in detailed gas dynamic and atom-trajectory Monte Carlo simulations, which results we present and discuss below in the next sections. The gas dynamic simulations of the buffer gas flow inside the gas cell and in the supersonic argon carrier gas jet we made have using the VARJET code. This code is based on the solution of a full system of time dependent Navier–Stokes equations and described in detail in [39]. The results of the gas dynamic simulations (flow fields of the buffer gas velocity, density and temperature) we then used in atom-trajectory Monte Carlo simulations.

Similar computer simulations we were also making earlier for different ion beams cooling and bunching in helium buffer gas flows, and their results presented elsewhere (e.g. see [17-19, 40-48]). Note, that our calculation results (gas dynamic + Monte Carlo) for ions extracted from the gas jet into vacuum are in a good agreement with the measurements (see e.g. [43, 44]). Based on our gas dynamic calculations, setups of gas-jet internal targets [49, 50] have been created. These calculations are in a good agreement with measured parameters and structure of the supersonic gas jets, as well.

For simplicity, at comparison of two mentioned above in-gas-jet techniques, the conventional one, which is using in the project JetRIS, we will refer below to as a "GSI nozzle" and the proposed here new technique as a "double-nozzle".

2. Results for GSI Nozzle

Schematic views of the JetRIS setup are presented in the both [32] and [33] articles (see Figure 1 there).

Three different nozzles, which cross sectional profiles shown in the Figure 3 in [33], were used at JetRIS setup in offline test measurements of neutral ^{164}Dy atoms fluorescence induced by one-step laser excitation. All these nozzles have the same throat diameter of 1 mm, but different length and contour of diverging supersonic part. The authors of [33] note, that these three nozzles were designed for different stagnation pressure in the gas cell (P_{cell}) and background pressure (P_{bg}) in the vacuum chamber of the gas jet expansion, we will refer to as a gas-jet chamber. The sophisticated contours of the left and right nozzles (see Figure 3 in Ref. [33]) were designed (Ref. [35]) and produced in KU Leuven, but due to the lack of exact information available to us about these nozzle's profiles, we could not use these two nozzles in our gas dynamic simulations. Contrary, the third nozzle, shown in the middle of Figure 3 (Ref. [33]) and referred to as "mid-range nozzle", has a simple conical diverging part with the length of 20 mm.

The authors of work [33] note, "The mid-range nozzle seems to be the best overall choice, since its resolution and homogeneity are both close to the optimal values found for the other two nozzles".

Preprints (www.preprints.org) | NOT PEER-REVIEWED | Posted: 12 April 2023 doi:10.20944/preprints202304.0251.v1

This is an additional reason why we chose this particular nozzle for a detailed computer study of the operation of the JetRIS setup.

The gas dynamic simulation we have performed for the argon stagnation pressure in the gas cell P_{cell} = 100 mbar and background pressure in the vacuum gas-jet chamber is $P_{bg} = 6.47 \cdot 10^{-3}$ mbar. The same pressure values were in JetRIS setup during test fluorescent measurements of neutral ^{164}Dy atoms inside the supersonic argon jet (see Table 1 and the Figure 4 caption in [33]).

2.1. The Exit Flow Channel

The JetRIS gas cell technical drawing shown in the left part of the Figure 5 in [32]. The inner diameter of the gas cell DC-cage is 160 mm with the length of 164.5 mm. The total length of DC-funnel (five electrodes having gradually decreasing diameters) placed behind the DC-cage is 63.5 mm. The exit flow channel placed between the DC-funnel and the nozzle have diameter of 12 mm and a length of 34.6 mm. Due to the large diameter of DC-cage (160 mm) and only of 1 mm the nozzle throat diameter, the average velocity of the gas flow inside the DC-cage is only about 8 mm/s. That is why it is necessary to use the DC gradient field inside the cell to speed up the transport of the decelerated radioactive ions.

Early, we were making detailed (gas dynamic + Monte Carlo) simulations for different big-sized gas stopping cells [6, 17 -19]. E.g., the results of our simulations for the UNICELL project [51], which is also under development at GSI presented in [17]. But here we should notice, that simulations of the ^{164}Dy ions transport through the main body of the JetRIS gas cell having inner diameter of 160 mm to the hot filament installed in-side the exit flow channel have been carefully done by the authors of [32]. But here we should notice, that simulations of the 164Dy ions transport through the main body of the JetRIS gas cell having inner diameter of 160 mm to the hot filament installed in-side the exit flow channel have been carefully done by the authors of [32]. Therefore, it is no much sense to repeat it, and we decided to start our gas dynamic simulation from the entrance to this exit flow channel (12 mm in diameter), where the average gas velocity in a factor of 178 higher than it is inside the DC-cage region. Notice, that the evaporated from the surface of hot filament neutral atoms are moving through the exit flow channel and then through the nozzle into the vacuum gas-jet chamber only under the effect of the gas flow. Monte Carlo atom-trajectory simulations were beginning from the filament tip, where neutral ^{164}Dy atoms first appear in the gas flow after their evaporation. From the technical drawing shown in the left part of the Figure 5 of work [32] we determined that the filament in the JetRIS setup has installed at about 22.5 mm distance from the nozzle.

Results of the gas dynamic simulation for the gas velocity flow field inside the exit flow channel shown in Figure 1.

The Figure 2 shows the radial gas velocity profile in the middle of this exit flow channel. The parabolic gas velocity profile, that is typical for the laminar viscous gas flow inside a tube, is clear visible. The corresponding Reynolds number is equal to 123.

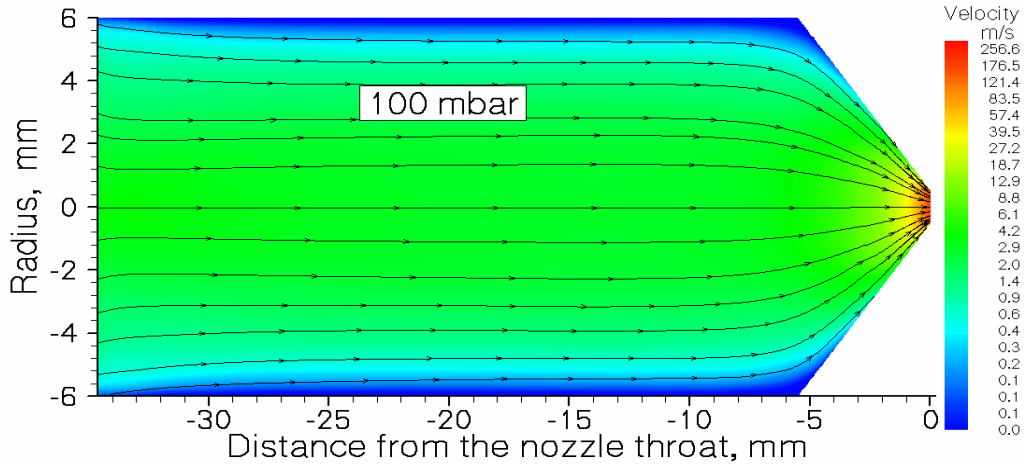

Preprints (www.preprints.org) | NOT PEER-REVIEWED | Posted: 12 April 2023 doi:10.20944/preprints202304.0251.v1

Figure 1. Results of the gas dynamic simulation for the argon velocity flow field inside the exit flow channel. The stagnation pressure P_{cell} = 100 mbar, the temperature of the channel walls T_{cell} = 296 K. The arrowed black lines show the gas flow direction.

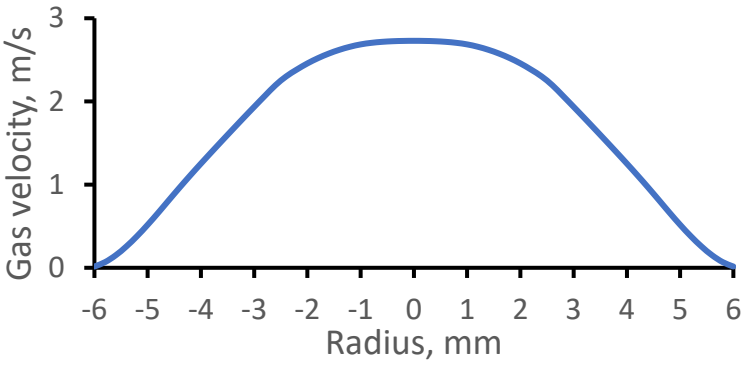

Figure 2. The calculated radial gas velocity profile in the middle of the exit flow channel.

Calculation results for the time-of-flight distribution ^{164}Dy atoms from the filament tip to the nozzle throat shown in Figure 3. The average atoms' extraction time is T = 7.0 ms, the time spread determined as full width at half maximum (FWHM) is ΔT = 1.4 ms. The corresponding extraction efficiency of ^{164}Dy atoms from the exit flow channel is (94,5 ± 2.7) %.

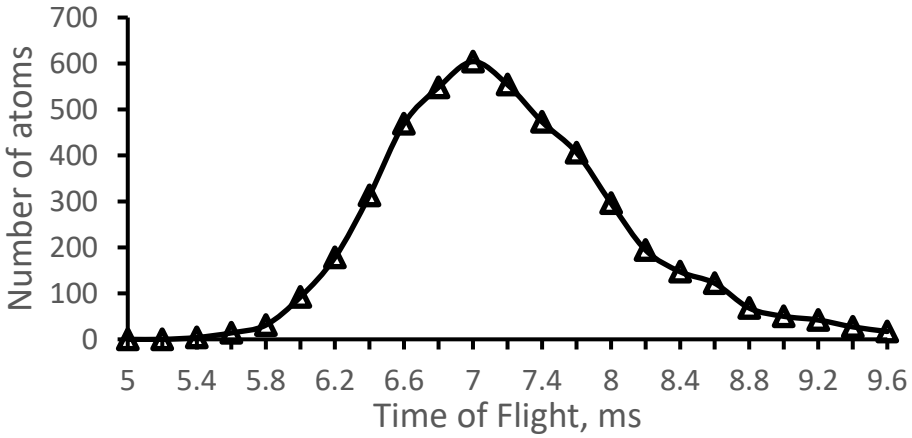

Figure 3. The time-of-flight of ^{164}Dy atoms from the filament tip to the nozzle throat. Total number of calculated atoms is 5000.

2.2. GSI Nozzle at Gas Cell Pressure P_{cell} = 100 Mbar and $P_{bg} = 6.47 \cdot 10^{-2}$ Mbar

Results of the gas dynamic simulation for argon gas density, temperature, velocity and Mach number flow fields for GSI nozzle are shown in Figure 4.

Preprints (www.preprints.org) | NOT PEER-REVIEWED | Posted: 12 April 2023 doi:10.20944/preprints202304.0251.v1

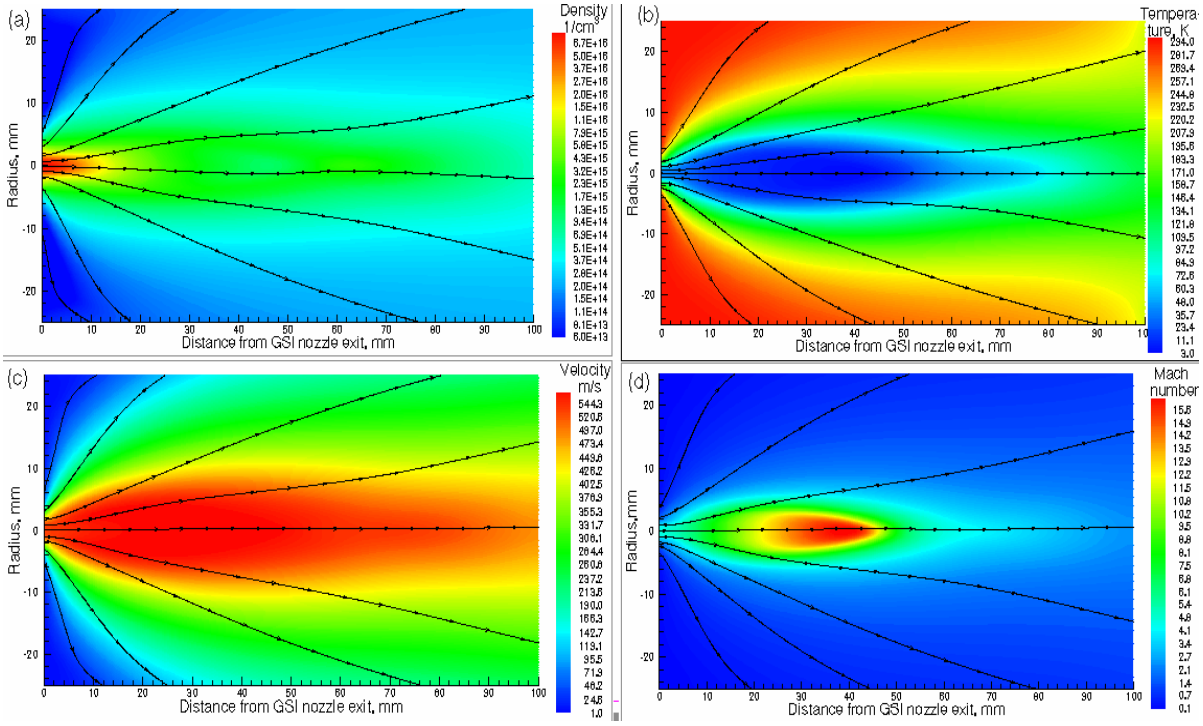

Figure 4. Results of the gas dynamic simulation for GSI nozzle: (a) density, (b) temperature, (c) velocity and (d) Mach number flow fields. The stagnation pressure and temperature in the gas cell are P_{cell} = 100 mbar and T_{cell} = 296 K, correspondingly. Background pressure in the vacuum gas-jet chamber is $P_{bg} = 6.47 \cdot 10^{-3}$ mbar. Black arrowed lines show the gas flow directions.

The results of gas dynamic simulation shown in Figure 4 we have used for Monte Carlo simulations of ^{164}Dy atomic beam. These results are presented in the next four Figures. The calculated fraction of the extracted from the gas cell ^{164}Dy atomic beam inside the region of 10 mm in diameter (it is the Laser-1 diameter in [33]) as a function of distance from GSI nozzle exit, shown in Figure 5. The decreasing of the dysprosium atomic beam fraction with the distance from GSI nozzle is simply explained by the gas jet divergence. The atomic beam diffusion losses inside GSI nozzle are equal to (15.6 ± 0.6) % and they are taken into account in the data presented in Figure 5.

Figure 6 demonstrates how the calculated longitudinal velocity spread of dysprosium atomic beam depends on the distance from GSI nozzle. The data averaged in the radial plane over the Laser-1 beam diameter, and this makes it possible to directly and simply compare our calculations with the future experiments at JetRIS setup. Moreover, such calculations allow for getting important quantitative information on a quality of the cooled in the supersonic gas jet atomic beams.

Preprints (www.preprints.org) | NOT PEER-REVIEWED | Posted: 12 April 2023 doi:10.20944/preprints202304.0251.v1

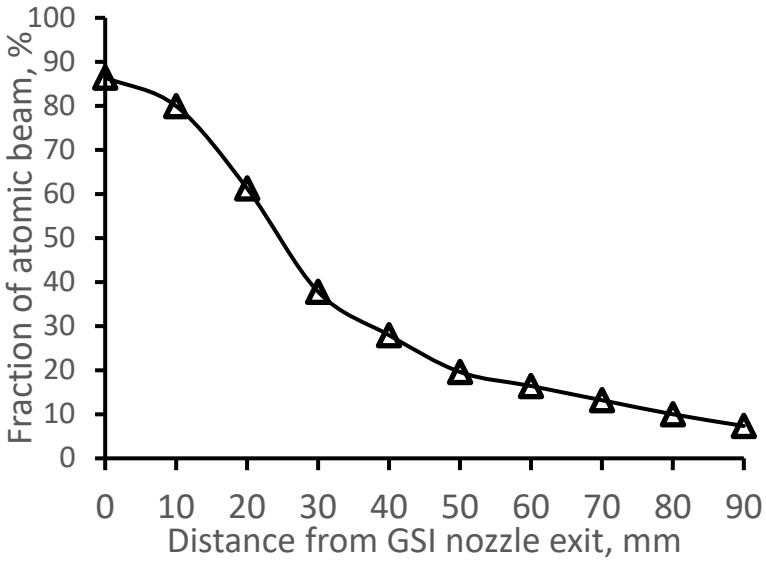

Figure 5. Results of the Monte-Carlo trajectory simulations of the fraction of the extracted from the gas cell ^{164}Dy atomic beam inside the region of 10 mm in diameter (it is the Laser-1 beam diameter) as a function of distance from GSI nozzle exit. Number of calculated atoms is 10000. .

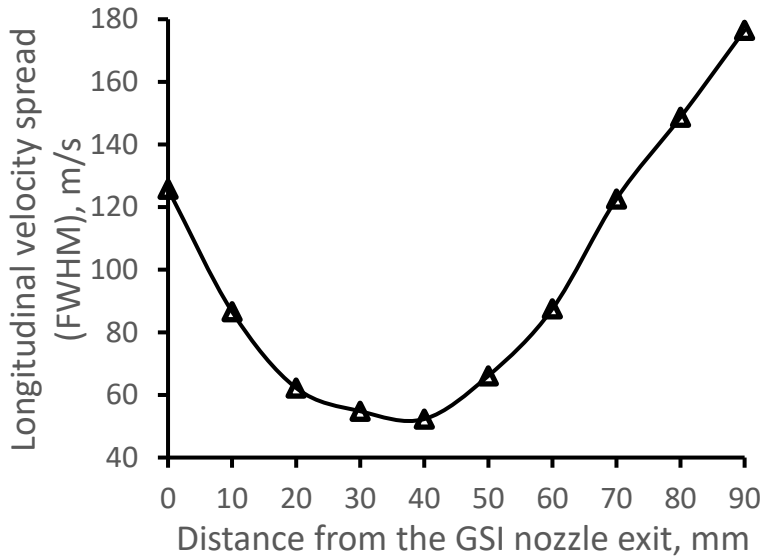

Figure 6. Results of the Monte-Carlo trajectory simulations for ^{164}Dy atomic beam longitudinal velocity spread (FWHM) as a function of the distance from GSI nozzle exit. The data averaged in the radial plane for the Laser-1 beam diameter of 10 mm. Number of calculated atoms is 10000.

Figure 7 and Figure 8 illustrate the distributions of longitudinal and radial ^{164}Dy atomic beam velocity components (averaged in the radial plane for the Laser-1 beam diameter of 10 mm) for different distances from GSI nozzle.

Preprints (www.preprints.org) | NOT PEER-REVIEWED | Posted: 12 April 2023 doi:10.20944/preprints202304.0251.v1

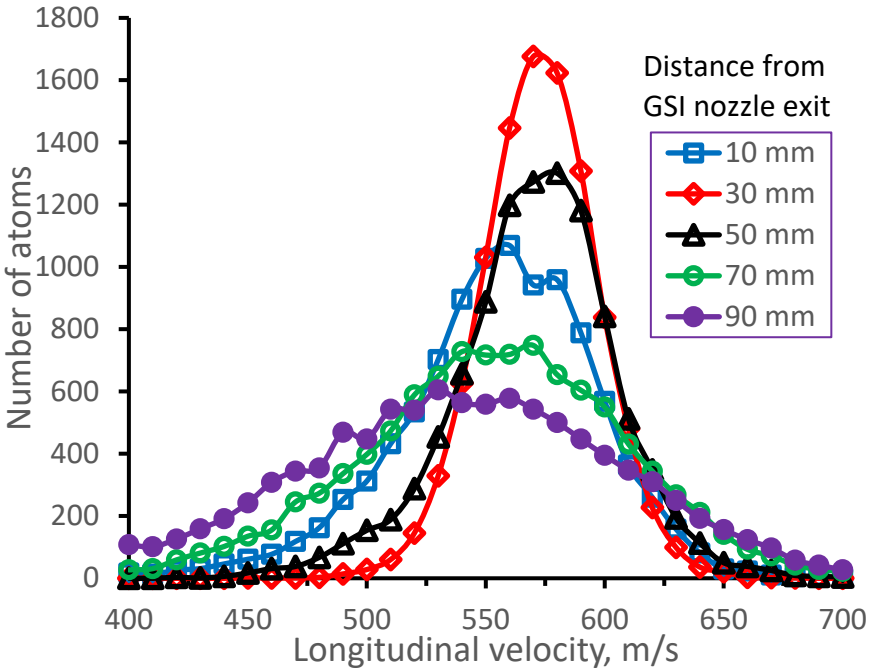

Figure 7. Results of the Monte-Carlo trajectory simulations for ^{164}Dy atomic beam longitudinal velocity distributions (averaged in the radial plane for the Laser-1 beam diameter of 10 mm) for different distances from GSI nozzle exit. Number of calculated atoms for each velocity distribution is 10000.

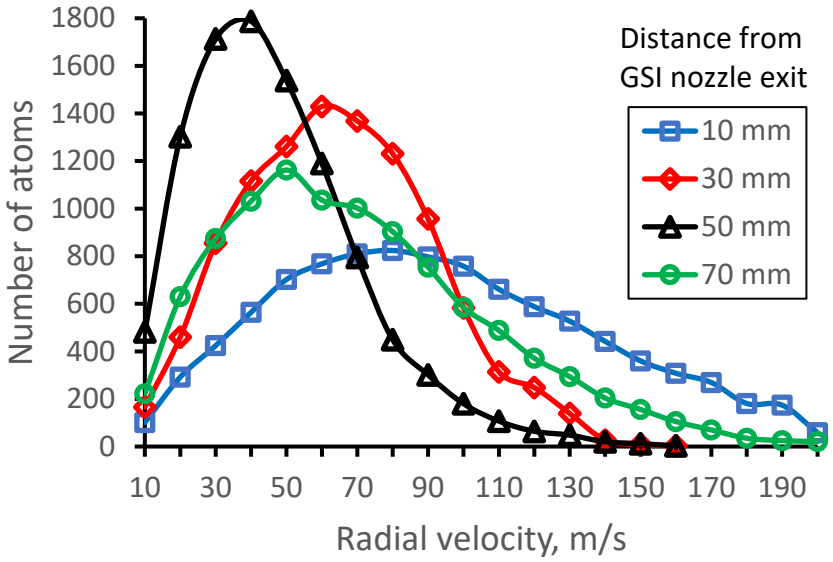

Figure 8. Results of the Monte-Carlo trajectory simulations for ^{164}Dy atomic beam radial velocity distributions (averaged in the radial plane for the Laser-1 beam diameter of 10 mm) for different distances from GSI nozzle exit. Number of calculated atoms for each velocity distribution is 10000.

2.3. GSI nozzle at gas cell pressure P_{cell} = 50 mbar and $P_{bg} = 3.23 \cdot 10^{-2}$ mbar

To check how the supersonic gas jet structure and parameters of extracted into the jet ^{164}Dy atomic beam will look at lower stagnation gas cell pressure, we performed calculations, which are similar to the calculations described above in the subection 2.2 for the same pumping capacity, but for the gas cell pressure of P_{cell} = 50 mbar. The results of the gas dynamic simulation for argon gas

Preprints (www.preprints.org) | NOT PEER-REVIEWED | Posted: 12 April 2023 doi:10.20944/preprints202304.0251.v1

density, temperature, velocity and Mach number flow fields for GSI nozzle at P_{cell} = 50 mbar are shown in Figure 9.

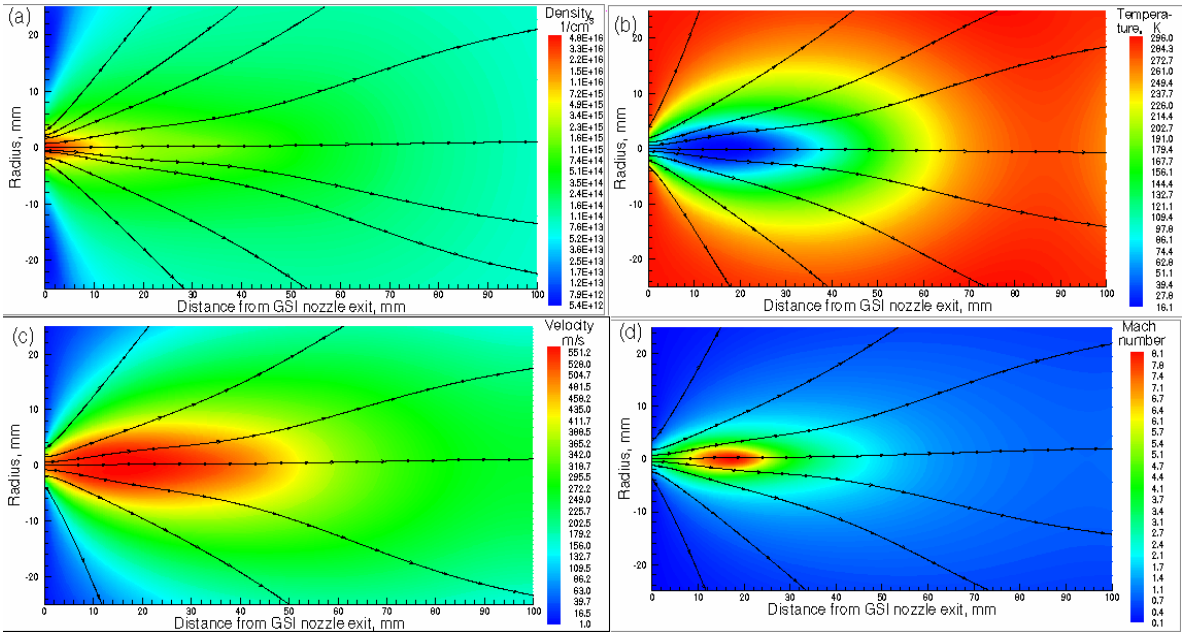

Figure 9. Results of the gas dynamic simulation: (a) density, (b) temperature, (c) velocity and (d) Mach number flow fields for GSI nozzle. The stagnation pressure and temperature in the gas cell are P_{cell} = 50 mbar and T_{cell} = 296 K, correspondingly. Background pressure in the gas-jet chamber is P_{bg} = $3.23 \cdot 10^{-3}$ mbar. Black arrowed lines show the gas flow directions.

Results of the Monte Carlo simulations for the case of 50 mbar gas cell pressure shown in Figures 10 and 11. We have included into these Figures results of calculations presented above in the Figures 5 and 6 for the case of P_{cell} = 100 mbar for comparison. Notice, that the atomic beam diffusion losses inside GSI nozzle at P_{cell} = 50 mbar is equal to (27.7 ± 0.8) % that is about factor 2 higher than that one at P_{cell} = 100 mbar.

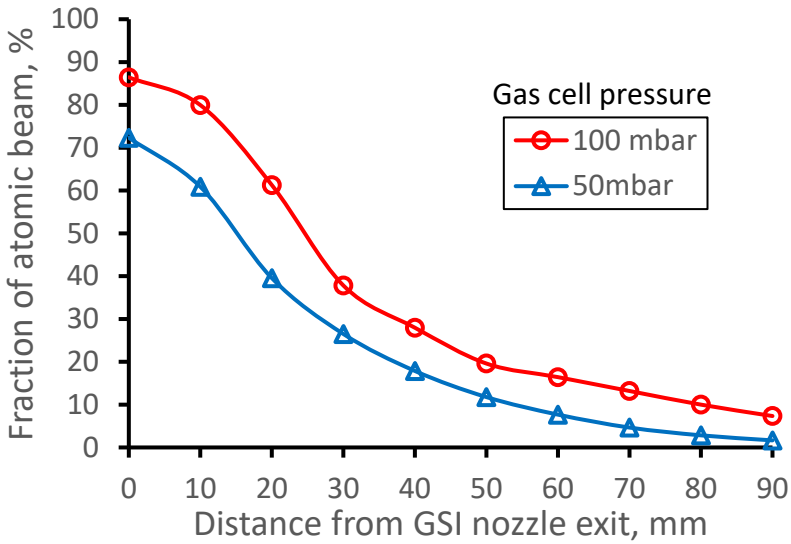

Figure 10. Results of the Monte-Carlo trajectory simulations of the fraction of the extracted from the gas cell ^{164}Dy atomic beam inside the region of 10 mm in diameter (it is the Laser-1 diameter) as a function of distance from GSI nozzle exit. Number of calculated atoms is 10000. .

Preprints (www.preprints.org) | NOT PEER-REVIEWED | Posted: 12 April 2023 doi:10.20944/preprints202304.0251.v1

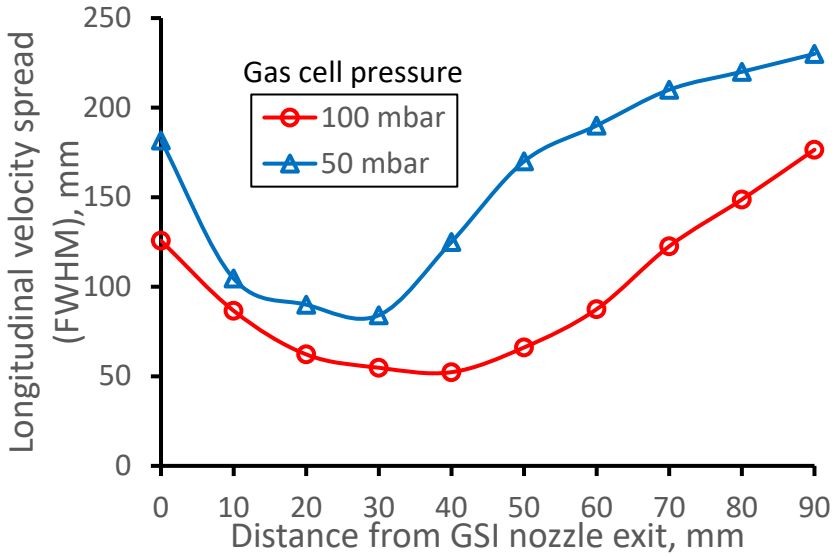

Figure 11. Results of the Monte-Carlo trajectory simulations for ^{164}Dy atomic beam longitudinal velocity spread (FWHM) as a function of distance from GSI nozzle exit. The data averaged in the radial plane for the Laser-1 beam diameter of 10 mm. Number of calculated atoms is 10000.

3. Results for double-nozzle technique

3.1. Historical notes

The new double-nozzle technique for in-gas-jet resonance ionization laser spectroscopy that we propose here is based on the idea of gas dynamic cooling of low-energy molecular and ion beams. This idea has been proposed for the first time in 1979 [52,53] and described also e.g. in [5, 39, 54–61]. It consists in direct injection of primary beams into supersonic carrier gas jet by the use of a specially designed supersonic nozzle. The converging–diverging supersonic nozzle has a narrow inner tube on its axis which passes through a gas stagnation chamber into a region of supersonic carrier gas expansion (see Figure 12). It is through this inner tube particles of interest are directly injected into the espanded supersonic gas jet. As a low-pressure zone forms immediately after the tube, this supersonic carrier gas jet acts as a vapor-jet pump and provides for the possibility of effective differential pumping in case of the ion beam injection [60].

To show experimentally the feasibility and effectivity of the described gas dynamic method, a setup of a gas dynamic molecular beam source has been constructed in the middle of 1980s in the Leningrad Nuclear Physics Institute (LNPI) in Gatchina [56,57]. In result of experimental investigations, it has been obtained the effective cooling of hot lead iodine (PbJ) molecular beam in the supersonic nitrogen jet from 900 K down to 20 K, and it was important part of our PhD work [54]. Notice, that the two-atomic molecules PbJ are free radicals, which produced via thermal decomposition of three-atomic molecules PbJ_2 inside the separatly heated thin quartz capillary installed into the inner tube of the supersonic nozzle shown in Figure 12.

The description, schematic layout with photos of some parts of this gas dynamic molecular beam source setup in LNPI one can find in our presentation at Institute for Medium Energy Physics (IMEP) (renamed after 2004 to “Stefan Meyer Institute” (SMI)), Vienna [61].

Preprints (www.preprints.org) | NOT PEER-REVIEWED | Posted: 12 April 2023 doi:10.20944/preprints202304.0251.v1

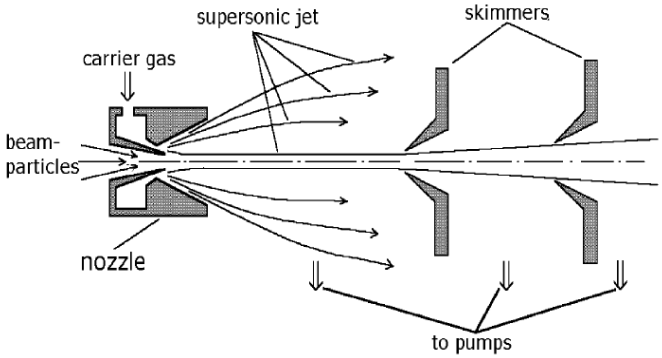

Figure 12. Schematic of the method of gas dynamic cooling of low-energy molecular and ion beams. Picture from Refs. [39, 61]. See the text for details.

3.2. Double-nozzle design

To implement the proposed here double-nozzle technique for in-gas-jet laser resonance ionization spectroscopy, it is sufficient to connect the short conical convergent-divergent nozzle of the gas cell, which we will call the 1st nozzle, with the 2nd nozzle, which design schematically shown in Figure 12.

Schematic views of the double-nozzle design combined with results of the gas dynamic simulation for argon temperature and velocity flow fields are shown in Figure 13 and Figure 14, correspondingly.

A gas vortex that one can clear see in Figures 13 and 14 appears in the region between the 1st nozzle throat and the exit of the inner tube in the 2nd nozzle due to the viscous gas jet interaction with the walls. This vortex around the supersonic jet flowing out the gas cell protects the dysprosium atoms from hitting the walls, thus reducing the diffusion losses of the neutral atomic beam extracted from the gas cell. The result of Monte Carlo calculation shows that only (9.5 ± 0.4) % of the extracted from the gas cell atomic beam is lost inside this double-nozzle device.

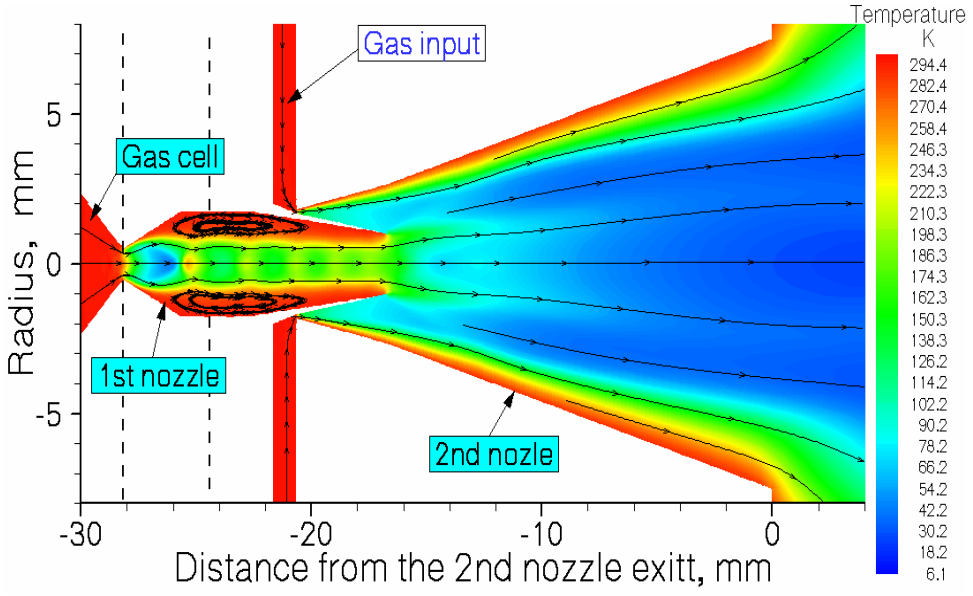

Figure 13. Schematic view of the double-nozzle design combined with results of the gas dynamic simulation for argon temperature flow field. The stagnation gas cell pressure P_{cell} = 100 mbar, gas input (stagnation) pressure P_{noz} = 81 mbar, background presse in the vacuum gas-jet chamber P_{bg} = $2.0 \cdot 10^{-2}$ mbar for the pumping capacity of 1300 l/s. The temperature of the gas cell and the both nozzles is 296 K. Black arrowed lines show the gas flow directions. Two black dashed vertical lines designate a possible connection of flanges for assembling this double-nozzle device.

Preprints (www.preprints.org) | NOT PEER-REVIEWED | Posted: 12 April 2023 doi:10.20944/preprints202304.0251.v1

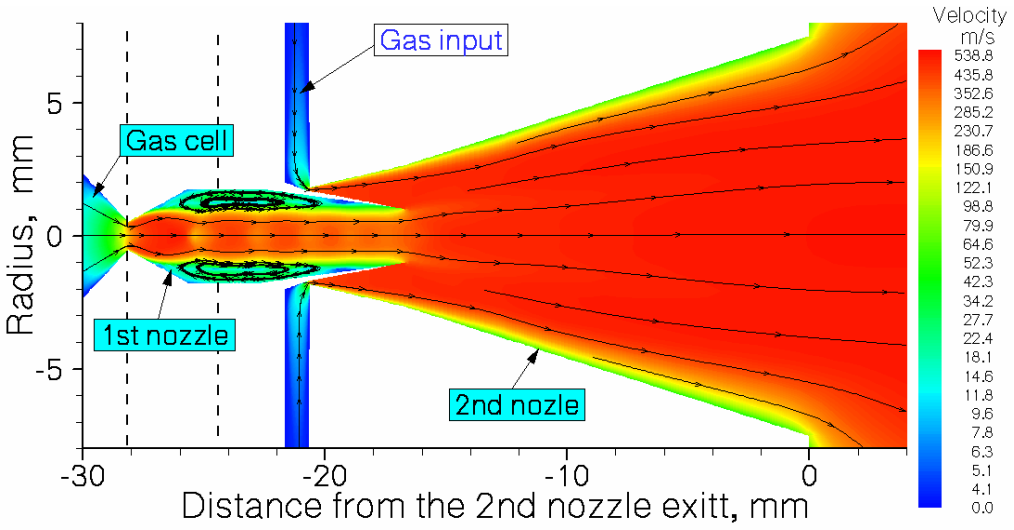

Figure 14. Schematic view of the double-nozzle design that shown in Figure 10, but combined with results of the gas dynamic simulation for argon velocity flow field.

Main design parameters of the double-nozzle device used in simulations listed in Table 1.

Table 1. Main design parameters of the double-nozzle device.

1st nozzle	
Exit diameter	3.5 mm
Throat diameter	1.0 mm
Length of diverging cone	2.5 mm
Connection tube between the 1st and 2nd nozzle	
Tube diameter	3.5mm
Tube length	3.0 mm
Inner tube in the 2nd nozzle	
Exit diameter	2.0 mm
Inner entrance diameter	3.5 mm
Inner total length	6.0 mm
Supersonic part length	4.0 mm
Out entrance diameter	4.0 mm

Preprints (www.preprints.org) | NOT PEER-REVIEWED | Posted: 12 April 2023 doi:10.20944/preprints202304.0251.v1

Outer total length	5.0 mm
Diverging 2nd nozzle	
Throat diameter	3.6 mm
Diverging cone length	20. mm
Exit diameter	15.0 mm
Annual gap between nozzle throat and inner tube	0.1 mm

3.3. Double-nozzle at P_{cell} = 100 mbar, P_{noz} = 81 mbar and P_{bg} = 2·10^{-2} mbar

Results of the gas dynamic simulation for argon gas density, temperature, velocity and Mach number flow fields for the double-nozzle shown in Figure 15.

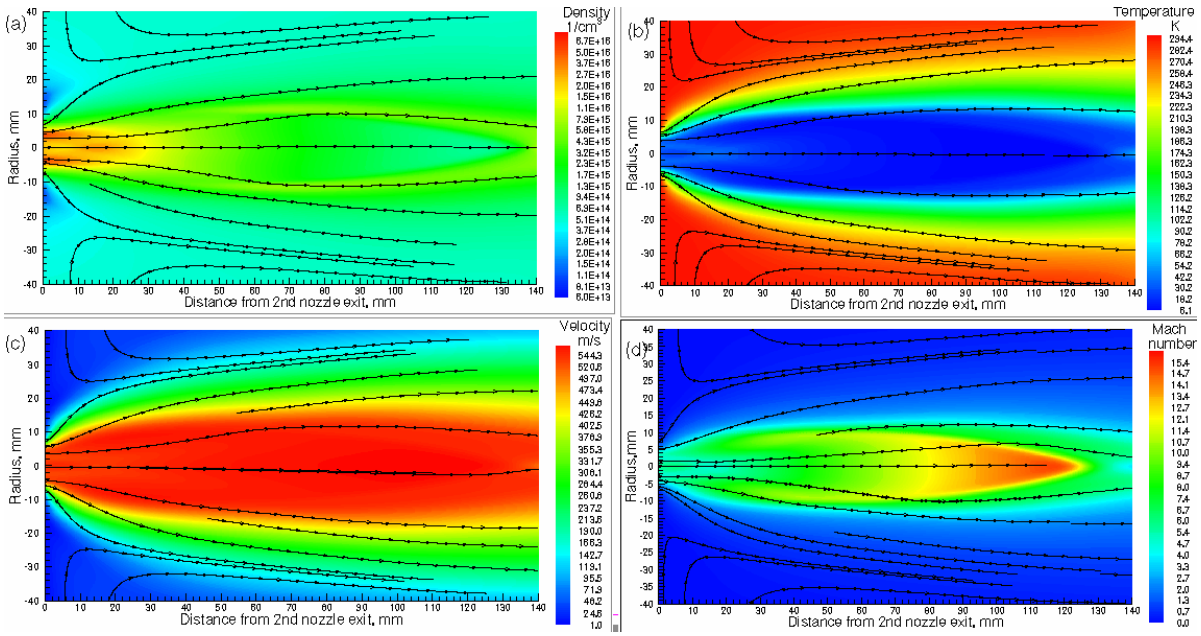

Figure 15. Results of the gas dynamic simulation: (a) density, (b) temperature (c) velocity and (d) Mach number flow fields for the double-nozzle. The stagnation gas cell pressure P_{cell} = 100 mbar, gas input (stagnation) pressure P_{noz} = 81 mbar, background pressure in the vacuum gas-jet chamber P_{bg} = 2.0·10^{-2} mbar for the pumping capacity of 1300 l/s. The temperature of the gas cell and the both nozzles is 296 K. Black arrowed lines show the gas flow direction.

Results of the Monte-Carlo simulations for the ^{164}Dy atomic beam extracted from the gas cell with the use of the double-nozzle technique, shown in Figures 16 - 19.

Preprints (www.preprints.org) | NOT PEER-REVIEWED | Posted: 12 April 2023 doi:10.20944/preprints202304.0251.v1

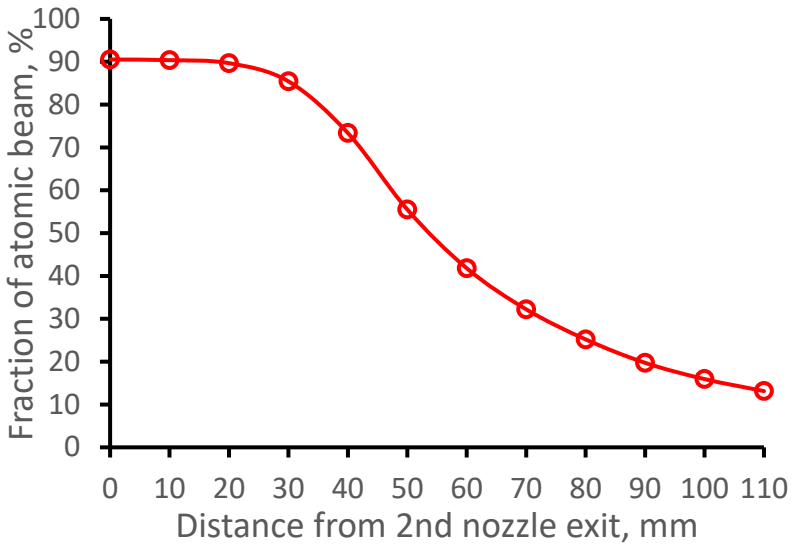

Figure 16. Results of the Monte-Carlo trajectory simulations of the fraction of the extracted from the gas cell ^{164}Dy atomic beam inside the gas jet of 10 mm in diameter (it is the Laser-1 diameter) as a function of distance from the 2nd nozzle exit. Number of calculated atoms is 10000. .

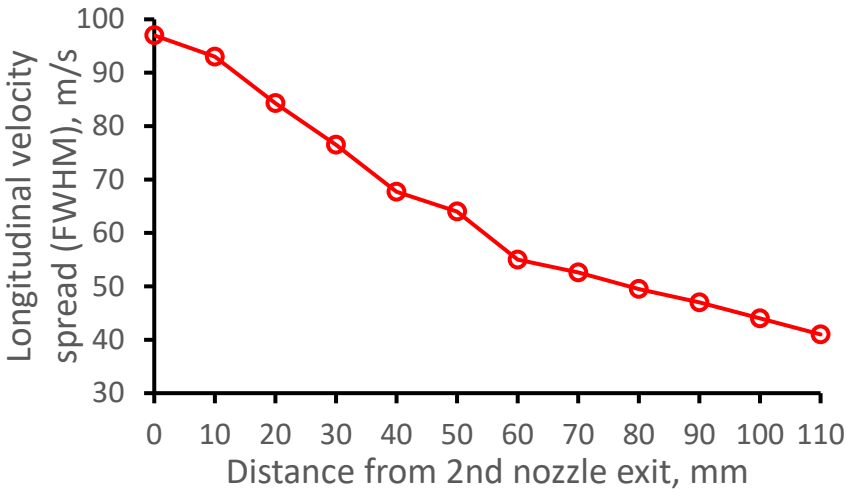

Figure 17. Results of the Monte-Carlo trajectory simulations for ^{164}Dy atomic beam longitudinal velocity spread (FWHM) as a function of the distance from the 2nd nozzle exit. The data averaged in the radial plane for the Laser-1 beam diameter of 10 mm. Number of calculated atoms is 10000.

Preprints (www.preprints.org) | NOT PEER-REVIEWED | Posted: 12 April 2023 doi:10.20944/preprints202304.0251.v1

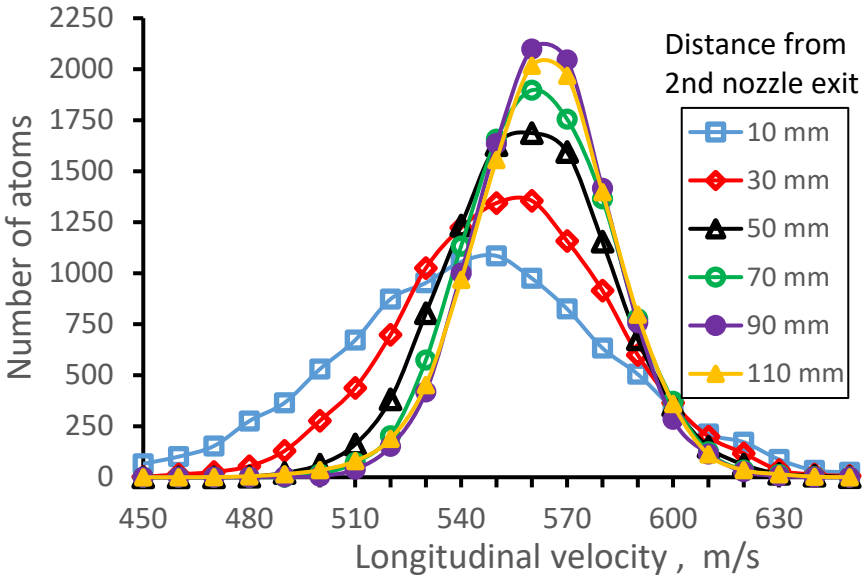

Figure 18. Results of the Monte-Carlo trajectory simulations for ^{164}Dy atomic beam longitudinal velocity distributions (averaged in the radial plane for the Laser-1 beam diameter of 10 mm) for different distances from 2nd nozzle exit. Number of calculated atoms for each velocity distribution is 10000.

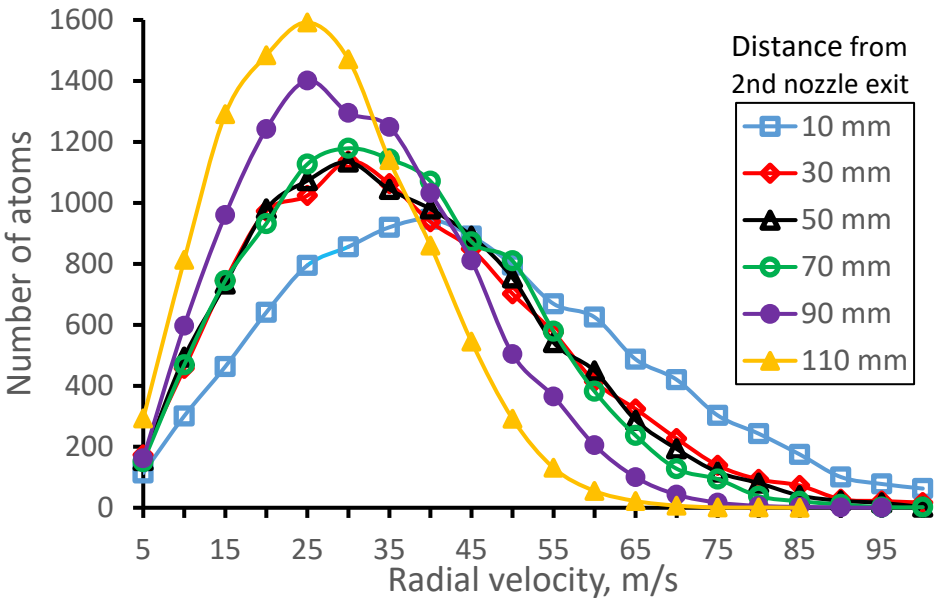

Figure 19. Results of the Monte-Carlo trajectory simulations for ^{164}Dy atomic beam radial velocity distributions (averaged in the radial plane for the Laser-1 beam diameter of 10 mm) for different distances from 2nd nozzle exit. Number of calculated atoms for each velocity distribution is 10000.

3.4. Effect of the pumping speed.

To investigate the effect of the pumping speed on the ^{164}Dy atomic beam parameters in the supersonic gas jet at fixed stagnation pressures P_{cell} = 100 mbar, P_{noz} = 81 mbar we have made corresponding gas dynamic and Monte Carlo simulations.

In addition to the previously considered variant of 1300 l/s pumping speed (it corresponds to $P_{bg} = 2 \cdot 10^{-2}$ mbar) we have performed calculations for the pumping speed of 2600 l/s ($P_{bg} = 1 \cdot 10^{-2}$ mbar) and 650 l/s ($P_{bg} = 4 \cdot 10^{-2}$ mbar). Results of these calculations presented in following Figures 20, 21 and 22. In order to provide a simple and direct comparison of the double-nozzle technique with the case

Preprints (www.preprints.org) | NOT PEER-REVIEWED | Posted: 12 April 2023 doi:10.20944/preprints202304.0251.v1

of GSI nozzle, we have included into these Figures results of calculations for GSI setup [32, 33] presented above in the section 2.

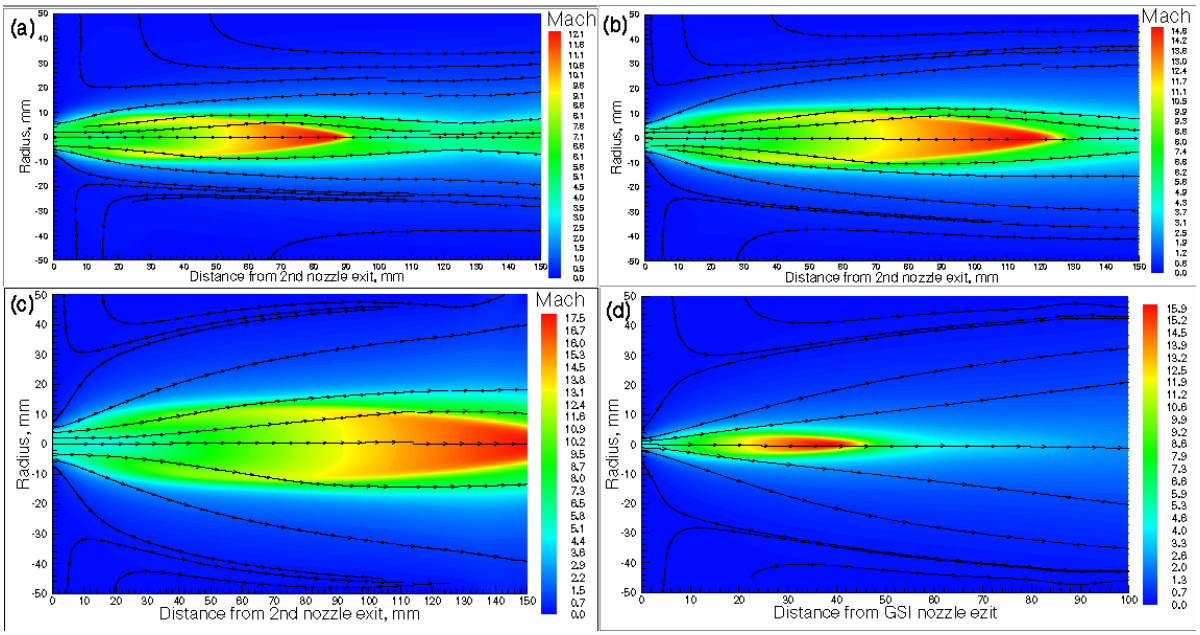

Figure 20. Results of the gas dynamic simulation for Mach number flow fields for double nozzle at different pumping speeds: (a) 650 l/s, (b) 1300 l/s, (c) 2600 l/s, (d) GSI nozzle. The stagnation gas cell pressure P_{cell} = 100 mbar, gas input (stagnation) pressure P_{noz} = 81 mbar. The temperature of the gas cell and the both nozzles is 296 K. Black arrowed lines show the gas flow direction.

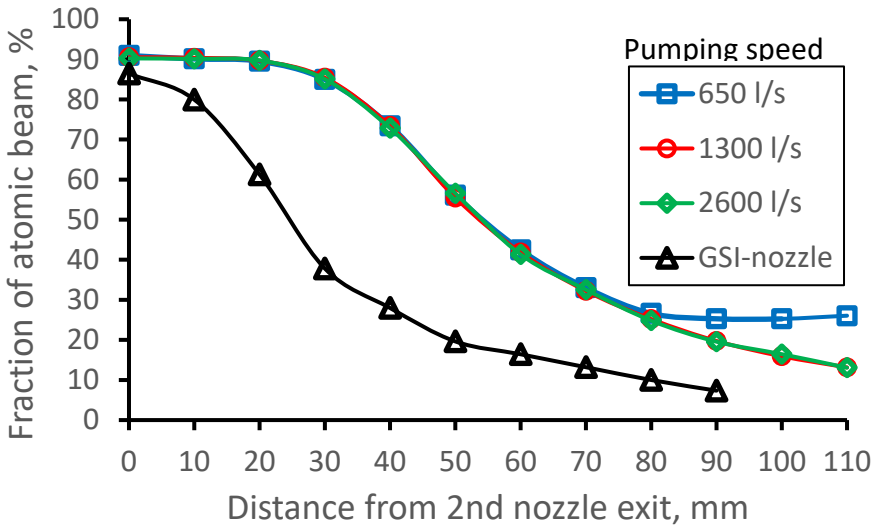

Figure 21. Results of the Monte-Carlo trajectory simulations of the fraction of the extracted from the gas cell ^{164}Dy atomic beam inside the gas jet of 10 mm in diameter (it is the Laser-1 diameter) for different pumping speeds as a function of distance from the 2nd nozzle exit. Number of calculated atoms is 10000 for each variant. .

Preprints (www.preprints.org) | NOT PEER-REVIEWED | Posted: 12 April 2023 doi:10.20944/preprints202304.0251.v1

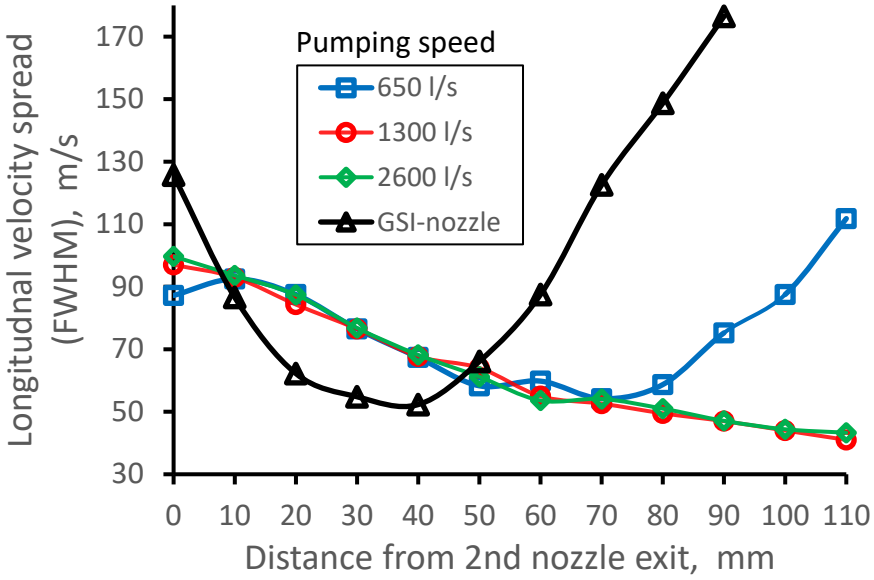

Figure 22. Results of the Monte-Carlo trajectory simulations for ^{164}Dy atomic beam longitudinal velocity spread (FWHM) for different pumping speeds as a function of the distance from the 2nd nozzle exit. The data averaged in the radial plane for the Laser-1 beam diameter of 10 mm. Number of calculated atoms is 10000 for each variant.

3.5. Effect of the input (stagnation) pressure in the 2nd nozzle

In order to make sure that the proposed here double-nozzle technique works effectively in a wide range of input pressures in the 2nd nozzle, we performed, in addition, gas dynamic and Monte Carlo simulations for two other pressures P_{noz} and at fixed gas cell pressure P_{cell} = 100 mbar and pumping capacity of 1300 l/s. These variants are P_{noz} = 162 mbar (the corresponding $P_{bg} = 3 \cdot 10^{-2}$ mbar) and P_{noz} = 263 mbar (the corresponding $P_{bg} = 4 \cdot 10^{-2}$ mbar).

Results of these Monte Carlo calculations presented in the Figures 23 and 24. The corresponding results for the case of GSI nozzle we added for illustration and comparison.

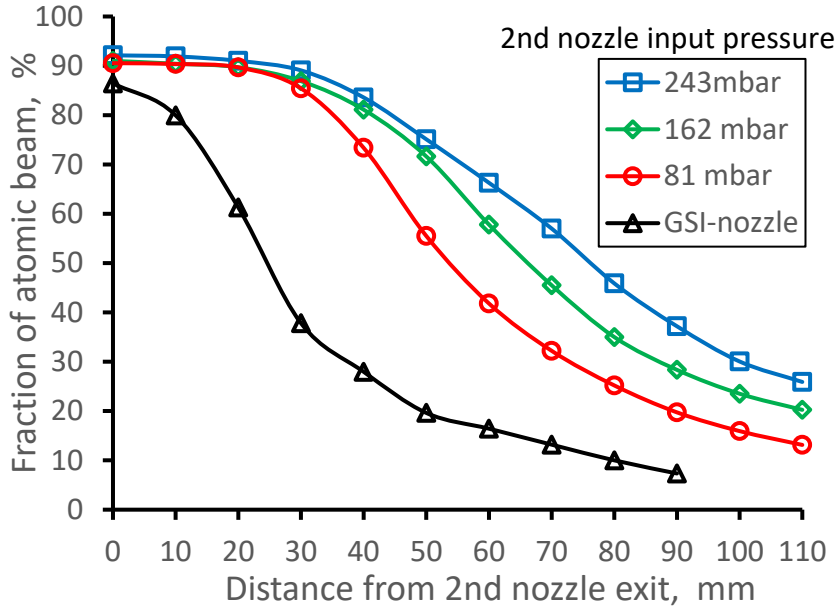

Figure 23. Results of the Monte-Carlo trajectory simulations of the fraction of the extracted from the gas cell ^{164}Dy atomic beam inside the region of 10 mm in diameter (it is the Laser-1 diameter) for

Preprints (www.preprints.org) | NOT PEER-REVIEWED | Posted: 12 April 2023 doi:10.20944/preprints202304.0251.v1

different input pressures P_{noz} as a function of distance from the 2nd nozzle exit. Number of calculated atoms is 10000 for each variant. .

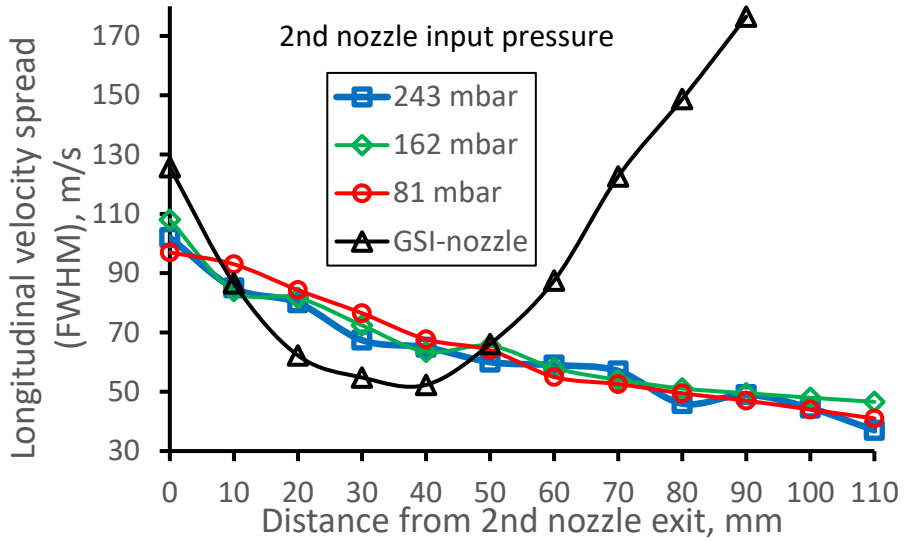

Figure 24. Results of the Monte-Carlo trajectory simulations for ^{164}Dy atomic beam longitudinal velocity spread (FWHM) for different input pressures P_{noz} as a function of the distance from the 2nd nozzle exit. The data averaged in the radial plane for the Laser-1 beam diameter of 10 mm. Number of calculated atoms is 10000 for each variant.

3.6. Effect of the stagnation pressure in the gas cell

To see how the double-nozzle technique will work at twice less stagnation pressure in the gas cell, we performed gas dynamic and Monte Carlo simulation for the case of P_{cell} = 50 mbar and input gas pressure P_{noz} = 81 mbar. For the pumping capacity of 1300 l/s it corresponds to $P_{bg} = 1.5 \cdot 10^{-2}$ mbar.

Results of this Monte Carlo calculation presented in Figures 25 and 26. The corresponding results for the previously considered case of stagnation P_{cell} = 100 mbar and $P_{bg} = 2 \cdot 10^{-2}$ mbar we added for illustration and comparison.

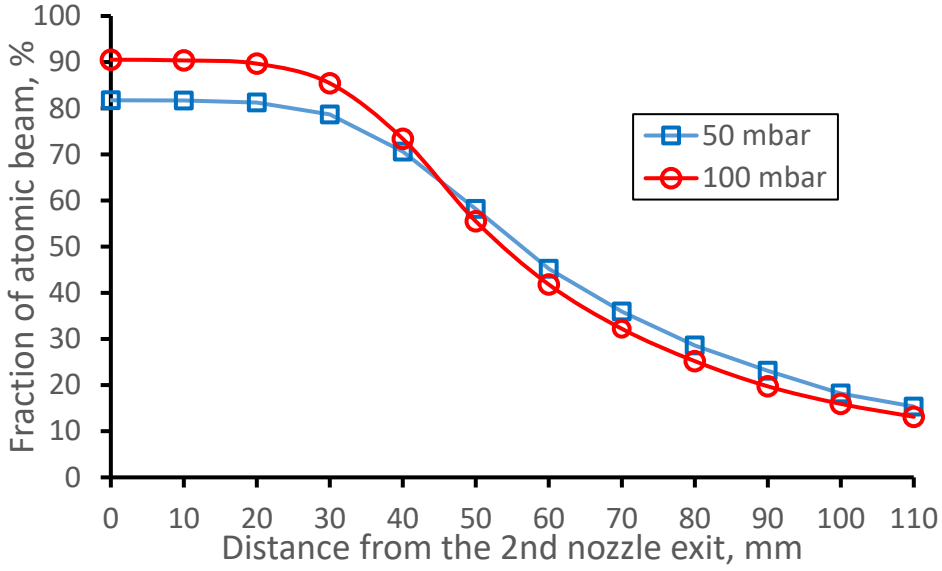

Figure 25. Results of the Monte-Carlo trajectory simulations of the fraction of the extracted from the gas cell ^{164}Dy atomic beam inside the region of 10 mm in diameter (it is the Laser-1 diameter) for two different gas cell pressures P_{cell} as a function of distance from the 2nd nozzle exit. Number of calculated atoms is 10000 for each variant. .

Preprints (www.preprints.org) | NOT PEER-REVIEWED | Posted: 12 April 2023 doi:10.20944/preprints202304.0251.v1

Notice that the calculated diffusion losses of the atomic beam inside the double-nozzle device at P_{cell} = 50 mbar is (18.3 ± 0.6) %, which in a factor of 2 higher than that one for P_{cell} = 100 mbar and it looks reasonable. Nevertheless, in general, the data for two different P_{cell} values look very similar in the both Figures 25 and 26. For comparison, it is not so for the case of GSI nozzle (see Figures 10 and 11).

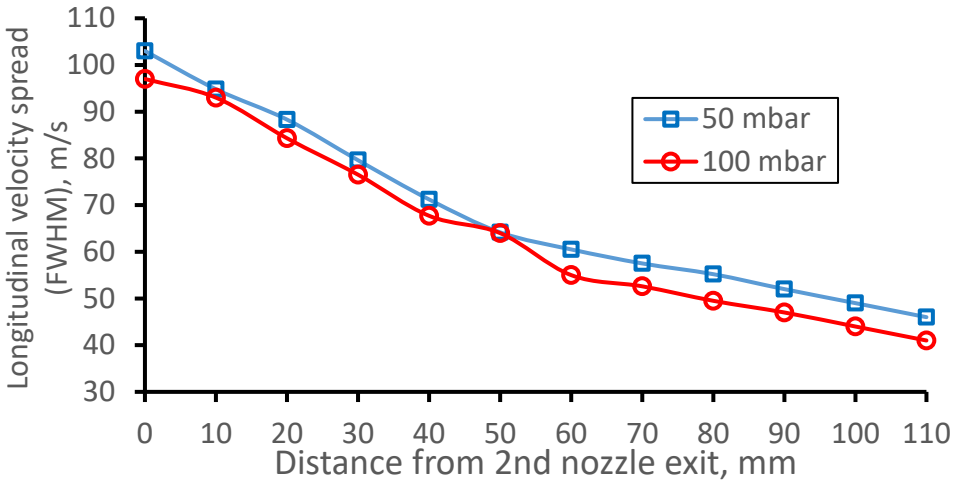

Figure 26. Results of the Monte-Carlo trajectory simulations for ^{164}Dy atomic beam longitudinal velocity spread (FWHM) for different input pressures P_{noz} as a function of the distance from the 2nd nozzle exit. The data averaged in the radial plane for the Laser-1 beam diameter of 10 mm. Number of calculated atoms is 10000 for each variant.

3.6. Effect of the Laser-1 beam diameter

When the distance between adjacent rods of the curved RFQ (the curved RFQ allows for the axial Laser-1 beam injection into the gas jet) less than considered above laser beam diameter of 10 mm, then one should use the Laser-1 beam of smaller diameter.

It is very important to know how the JetRIS (or any other similar project) overall efficiency and quality of the extracted into gas jet atomic beam depend on the Laser-1 beam diameter. Some information about one can get from results of our Monte Carlo simulations shown in the Figures 27 and 28.

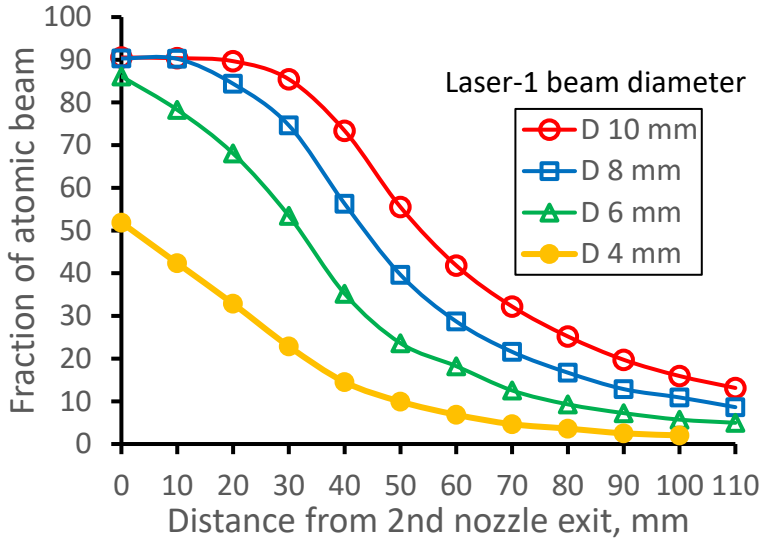

Figure 27. Results of the Monte-Carlo trajectory simulations of the fraction of the extracted from the gas cell ^{164}Dy atomic beam for different Laser-1 beam diameters as a function of distance from the 2nd nozzle exit. Number of calculated atoms is 10000 for each variant. .

Preprints (www.preprints.org) | NOT PEER-REVIEWED | Posted: 12 April 2023 doi:10.20944/preprints202304.0251.v1

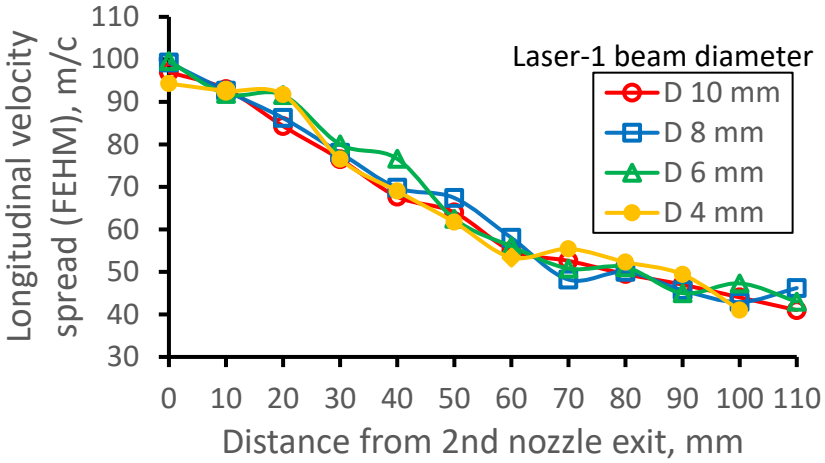

Figure 28. Results of the Monte-Carlo trajectory simulations for ^{164}Dy atomic beam longitudinal velocity spread (FWHM) for different Laser-1 beam diameters as a function of the distance from the 2nd nozzle exit. The data averaged in the radial plane for each Laser-1 beam diameter. Number of calculated atoms is 10000 for each variant.

3.7. Monte Carlo simulations for nobelium atoms in the gas jet.

The goal of the JetRIS project [32, 33] that is under development at GSI is the study of nuclear properties of nobelium isotopes with high precision by laser spectroscopy in argon supersonic gas jet. That is why we performed, in addition, Monte Carlo simulation for ^{253}No isotope, as well. For the Monte Carlo simulation of nobelium atomic beam in supersonic gas jet, we used the same results of gas dynamic simulation (see Figure 15) that we used for the ^{164}Dy atomic beam. These results shown in Figures 29, 30 and 31. Results for the ^{164}Dy we added for comparison.

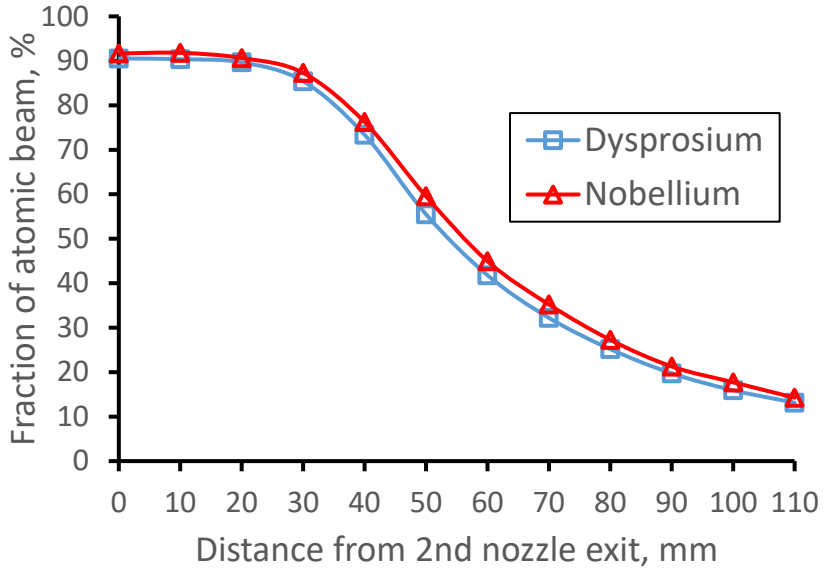

Figure 29. Results of the Monte-Carlo trajectory simulations of the fraction of the extracted from the gas cell ^{253}No atomic beam inside the gas jet of 10 mm in diameter (it is the Laser-1 diameter) for the gas cell pressure P_{cell} = 100 mbar, P_{noz} = 81 mbar and P_{bg} = $2{\cdot}10^{-2}$ mbar as a function of distance from the 2nd nozzle exit. Number of calculated atoms is 10000 for each case. .

Preprints (www.preprints.org) | NOT PEER-REVIEWED | Posted: 12 April 2023 doi:10.20944/preprints202304.0251.v1

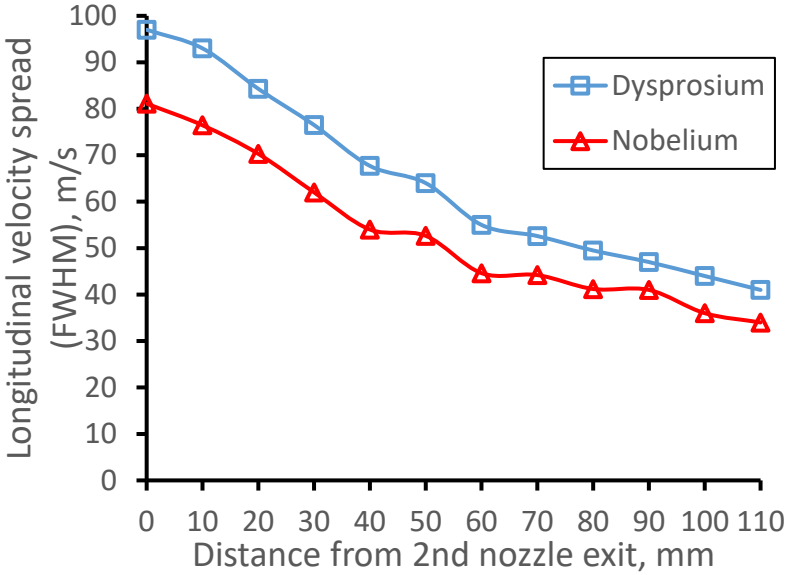

Figure 30. Results of the Monte-Carlo trajectory simulations for ^{253}No atomic beam longitudinal velocity spread (FWHM) for the gas cell pressure P_{cell} = 100 mbar, P_{noz} = 81 mbar and P_{bg} =2·10^{-2} mbar as a function of the distance from the 2nd nozzle exit. The data averaged in the radial plane for the Laser-1 beam diameter of 10 mm. Number of calculated atoms is 10000 for each case.

As one can see in Figure 29, the decrease of the beam fractions with the distance from the 2nd nozzle exit are near the same for the both dysprosium and nobelium atomic beams. It reflects the fact that thermalized in the argon dysprosium and nobelium atoms equally follow the supersonic jet expansion. At the same time, the longitudinal velocity spreads shown in Figure 30 are different. It explains by the mass difference of ^{164}Dy and ^{253}No atoms, because the velocity spread of the atomic beam thermalized in the gas should be inverse proportional to the square root of the atom mass.

In the Figure 31 the ^{253}No atomic beam longitudinal velocity distributions for different distances from 2nd nozzle exit shown for illustration.

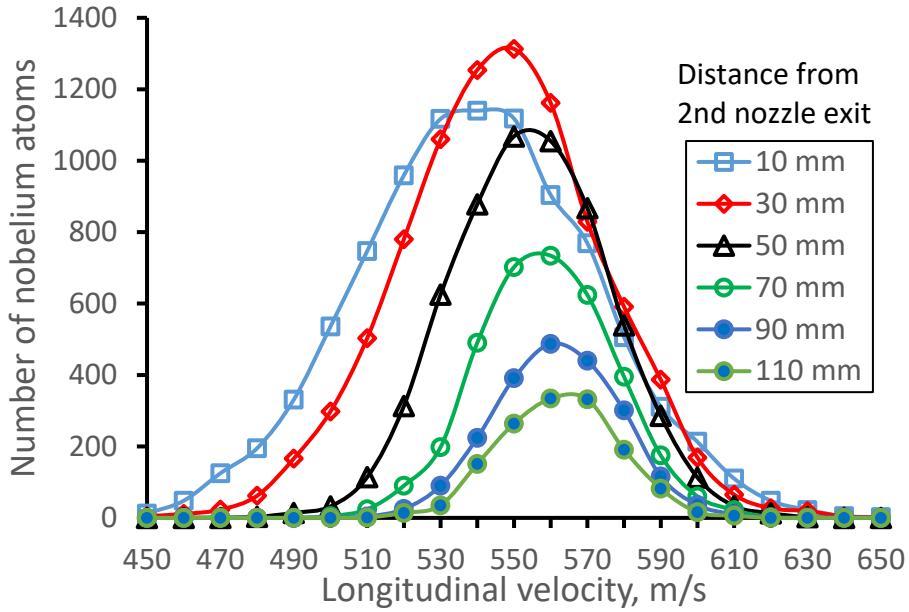

Figure 31. Results of the Monte-Carlo trajectory simulations for ^{253}No atomic beam longitudinal velocity distributions (averaged in the radial plane for the Laser-1 beam diameter of 10 mm) for different distances from 2nd nozzle exit. Number of calculated atoms for each velocity distribution is 10000.

 doi:10.20944/preprints202304.0251.v1

4. Discussion and outlook.

In the section 2 of the article, we have investigated by means of detailed computer experiments the conventional nowadays technique of the so-called in-gas-jet laser resonance ionization spectroscopy. As a typical representative of this technique, we have chosen for the numerical computer analysis the setup of the JetRIS project [32, 33]. The JetRIS project is under development now at GSI, Darmstadt.

Results of gas dynamic simulation for the exit flow channel of 12 mm in diameter presented in Figures 1 and 2. It is a laminar gas flow with Reynolds number of 123. The calculated in Monte Carlo simulation time-of-flight of evaporated 164Dy neutral atoms from the hot filament tip to the nozzle throat is (7.0 ± 1.4) ms (see Figure 3.), the extraction efficiency is (94.5 ± 2.7) %, or in other words the atomic beam diffusion losses are equal to (5.5 ± 0.3) %. The gas dynamic + Monte Carlo simulations shows that the additional diffusion losses of the 164Dy atomic beam inside GSI nozzle at P_{cell} =100 mbar are equal to (15.6 ± 0.6) %. The graphic description of the calculated argon supersonic jet (flow fields of gas density, velocity, temperature and Mach number) flowing out of GSI nozzle into the gas-jet chamber shown in Figure 4 and Figure 9 for the gas cell pressure of 100 mbar and 50 mbar, correspondingly. Here the strong effect of the gas viscosity of the supersonic jet structure and parameters is clear visible.

Notice that the 164Dy atomic beam diffusion losses inside GSI nozzle for P_{cell} = 50 mbar (27.7 ± 0.8) % are considerably higher than that one at P_{cell} = 100 mbar, and it looks reasonable. The production efficiency of excited by the Laser-1 dysprosium atoms in the gas jet is also less in the case of P_{cell} = 50 mbar (see Figure 10). The atomic beam quality, shown in Figure 11 as a longitudinal velocity spread, is also worse.

The section 3 of the article devoted to description and exploration of our proposal of a new double-nozzle technique. By means of gas dynamic and Monte Carlo simulations, we have shown that this new technique has many advantages over the conventional technique described in the section 2 of the article. E.g., the atomic beam diffusion losses inside the double-nozzle system are equal only to (9.5 ± 0.4) % that is in a factor 1.6 less than in the case of the use of GSI nozzle at the same gas cell pressure (P_{cell} = 100 mbar) and having the same nozzle throat diameter of 1.0 mm. The double nozzle method is much more efficient (see direct comparison in figures 16, 21 and 23) and it allows also obtaining better atomic beam quality (expressed in longitudinal velocity spread) for a longer downstream distance from the 2nd nozzle exit (see direct comparison in Figures 17, 22 and 24).

The proposed double-nozzle technique can effectively work in a wide range of P_{cell} and Pnoz pressures. There are no needs here for the use of any butterfly valve, placed in front of the vacuum pump, as it is in [32] to adjust the background pressure in the gas-jet chamber under changing the P_{cell}, or using the nozzles having different throat diameters and profiles of its diverging supersonic part. The butterfly valve allows decreasing the nominal capacity of the used vacuum pump, but it cannot increase it, when it is required.

Moreover, the same double-nozzle design, that we suggest for the use in JetRIS setup at GSI and which main parameters are listed in Table 1, can be effectively used at different vacuum pump capacities (see for details the subsection 3.4 above).

To help the authors of works [32, 33] in their preparation for the future online measurement of nobelium isotopes, we performed the Monte Carlo simulations for the 253No atomic beam in the argon supersonic jet, as well. The results of these calculations, which presented in the subsection 3.7, allow to quantitative estimate the efficiency of the JetRIS setup operation under the use in it the proposed double-nozzle technique.

To implement the proposed double-nozzle technique to the JetRIS setup, it will be enough just replace the present GSI nozzle by the double-nozzle system presented in the article.

In conclusion, we can say that the double-nozzle design, which main parameters are listed in the Table 1, can be also used for the other similar setups or/and projects. If, e.g., operation conditions or some specific requirements to these setups/projects are very differ of that one in the JetRIS setup, and

then we can make similar computer experiments to find an optimal solution for these cases upon the corresponding request.

Funding: This research received no external funding.

Data Availability Statement: The data presented in this study are available upon request from the corresponding author

Conflicts of Interest: The author declare no conflict of interest

References

1. Peter. Dendooven, Tthe development and status of the IGISOL technique, *Nucl. Instrum. Methods Phys. Res.* ***B 126*** *(1997) 182-189.*
2. Juha Äystö, Development and applications of the IGISOL technique, *Nucl. Instrum. Methods Phys. Res.* ***A 693*** *(2001) 477-494.*
3. I.D. Moore, P. Dendooven, J. Ärje, The IGISOL technique—three decades of developments, *Hyperfine Interact.* ***223*** *(2014) 17–62, http://dx.doi.org/10.1007/10751-013-0871-0.*
4. S. Schwarz, G. Bollen, D. Lawton, P. Lofy, D.J. Morrissey, J. Ottarson, R. Ringle, P. Schury, T. Sun, V. Varentsov, L. Weissman, The low-energy-beam and ion-trap facility at NSCL/MSU, *Nucl. Instrum. Methods Phys. Res.* ***B 204*** *(2003) 507-511.*
5. V.L. Varentsov, D. Habs, A cooler for intense low-energy ion beams, *Nucl. Instrum. Methods Phys. Res.* ***A 496*** *(2003) 286-292, http://dx.doi.org/10.1016/S0168-9002(02)01066-5.*
6. V.L. Varentsov, D. Habs, Fair-wind gas cell—a new concept of a buffer gas cell design, *Nucl. Instrum. Methods Phys. Res. A 490 (2002) 16-29, http://dx.doi.org/10.1016/S0168-9002(02)01761-8.*
7. Tetsu Sonoda, Masahiro Fujita, Akiyoshi Yamazaki, Takuya Endo, Tsutomu Shinozuka, Yuji Miyashita, Nozomi Sato, Atsushi Goto, Eiji Tanaka, Tomokazu Suzuki, Toru Miyake, Minoru Tanigaki, Michiharu Wada, Development of the RF-IGISOL at CYRIC, *Nucl. Instrum. Methods Phys. Res.* ***B 254*** *(2007) 295-299, http://dx.doi.org/10.1016/j.nimb.2006.10.084.*
8. I.D. Moore, New concepts for the ion guide technique, Nucl. Instrum. Methods Phys. Res. **B 266** (2008) 4434-4441.
9. T. Sonoda, M. Wada, H. Tomita, C. Sakamoto, T. Takatsuka, T. Furukawa, H. Iimura, Y. Ito, T. Kubo, Y. Matsuo, H. Mita, S. Naimi, S. Nakamura, T. Noto, P. Schury, T. Shinozuka, T. Wakui, H. Miyatake, A. Takamine, Development of a resonant laser ionization gas cell for high-energy, short-lived nuclei, *Nucl. Instrum. Methods Phys. Res.* ***B 295*** *(2013) 1-10, http://dx.doi.org/10.1016/j.nimb2012.10.009.*
10. P. Schury, M. Wada, Y. Ito, F. Arai, D. Kaji, S. Kimura, K. Morimoto, H. Haba, S. Jeong, H. Koura, H. Miyatake, K. Morita, M. Reponen, A. Ozawa, T. Sonoda, A. Takamine, H. Wollnik, Status of the low-energy super-heavy element facility at RIKEN, *Nucl. Instrum. Methods Phys. Res.* ***B 376*** *(2016) 425-428, http://dx.doi.org/10.1016/j.nimb.2016.02.061.*
11. K. Cooper, C.S. Sumithrarachchi, D.J. Morrissey, A. Levand, J.A. Rodriguez, G. Savard, S. Schwarz, B. Zabransky, Extraction of thermalized projectile fragments from a large volume gas cell, *Nucl. Instrum. Methods Phys. Res.* ***A 763*** *(2014) 543-546, http://dx.doi.org/10.1016/j.nima.2014.06.075.*
12. S. Schwarz, G. Bollen, S. Chouhan, J.J. Das, M. Green, C. Magsig, D.J. Morrissey, J. Ottarson, C. Sumithrarachchi, A.C.C. Villari, A. Zeller, The NSCL cyclotron gas stopper – Entering commissioning, *Nucl. Instrum. Methods Phys. Res.* ***B 376*** *(2016) 256-259, http://dx.doi.org/10.1016/j.nimb.2015.12.035.*
13. P. Constantin, D.L. Balabanski, L.T. Anh, P.V. Cuong, B, Design of the gas cell for the IGISOL facility at ELI-NP, *Nucl. Instrum. Methods Phys. Res.* ***B 397*** *(2017) 1-10, http://dx.doi.org/10.1016/j.nimb.2017.02.032.*
14. G. Savard, A.F. Levand, B.J. Zabransky, The CARIBU gas catcher, *Nucl. Instrum. Methods Phys. Res.* **A 685** *(2012) 70-77, http://dx.doi.org/10.1016/j.nima.2012.05031.*
15. A. Saastamoinen, I.D. Moore, M. Ranjan, P. Dendooven, H. Penttilä, K. Peräjärvi, A. Popov, J. Äystö, Characterization of a cryogenic ion guide at IGISOL, *Nucl. Instrum. Methods Phys. Res.* ***B 376*** *(2016) 246, http://dx.doi.org/10.1016/j.nimb.2016.02.050.*
16. M. Ranjan, P. Dendooven, S. Purushothaman, T. Dickel, M.P. Reiter, S. Ayet, E. Haettner, I.D. Moore, N. Kalantar-Nayestanaki, H. Geissel, W.R. Plaß, D. Schäfer, C. Scheidenberger, F. Schreuder, H. Timersma, J. Van de Walle, H. Weick, Design, construction and cooling system performance of a prototype cryogenic stopping cell for the super-FRS at FAIR, *Nucl. Instrum. Methods Phys. Res.* ***A 770*** *(2015) 87-97, http://dx.doi.org/10.1016/j.nima.2014.09.075.*

17. Victor Varentsov, AlexanderYakushev, Concept of a new Universal High-Density Gas Stopping Cell Setup for study of gas-phase chemistry and nuclear properties of Super Heavy Elements (UniCell), *Nucl. Instrum. Methods Phys. Res.* ***A*** **940** *(2019) 206-214, https://doi.org/10.1016/j.nima.2019.06.032.*
18. V.L. Varentsov and M. Wada, Computer experiments on ion beam cooling and guiding in fair-wind gas cell and extraction RF-funnel system, *Nucl. Instrum. Methods Phys. Res.* ***A*** **532** *(2004) 210, http://doi.org/10.1016/j.nima.2004.06.078.*
19. Victor Varentsov, AlexanderYakushev, Fair-wind gas cell for the UniCell setup, Nucl. Instrum. Methods Phys. Res. **A 1010** (2021) 165487, http://doi.org/10.1016/j.nima.2021.165487.
20. Ramzi Boussaid, G. Ban, G. Quéméner, Y. Merrer, and J. Lorry, Development of a radio-frequency quadrupole cooler for high beam currents, *Phys. Rev. Accel. Beams,* ***20****, (2017) 124701, https://doi.org/10.1103/PhysRevAccelBeams.20.124701.*
21. B.R. Barquest, G. Bollen, P.F. Mantica, K. Minamisono, R. Ringle, S. Schwarz, RFQ beam cooler and buncher for collinear laser spectroscopy of rare isotopes, *Nucl. Instrum. Methods Phys. Res. A* ***866*** *(2017) 18-28, https://doi.org/10.1016/j.nima.2017.05.036.*
22. S. Schwarz, G. Bollen, R. Ringle, J. Savory, P. Schury, The LEBIT ion cooler and buncher, *Nucl. Instrum. Methods Phys. Res.* ***A 816*** *(2017) 131-141, https://doi.org/10.1016/j.nima.2016.01.078.*
23. H. Franberg, P. Delahaye, J. Billowes, K. Blaum, R. Catherall, F. Duval, O. Gianfrancesco, T. Giles, A. Jokinen, M. Lindroos, D. Lunney, E. Mane, I. Podadera, Off-line commissioning of the ISOLDE cooler, *Nucl. Instrum. Methods Phys. Res.* ***A 266*** *(2008) 4502-4504, https://doi.org/10.1016/j.nimb.2008.05.097.*
24. B.R. Barquest, J.C. Bale, J. Dilling, G. Gwinner, R. Kanungo, R. Krücke, M.R. Pearson, Development of a new RFQ beam cooler and buncher for the CANREB project at TRIUMF, *Nucl. Instrum. Methods Phys. Res.* ***B 376*** *(2016) 207-210, https://doi.org/10.1016/j.nimb.2016.02.035.*
25. T. Brunner, M.J. Smith, M .Brodeur, S. Ettenauer, A.T .Gallant, V.V. Simon, A. Chaudhuri, A. Lapierre, E. Mane´, R. Ringle, M.C .Simon, J.A. Vaz, P. Delheij, M. Good, M.R. Pearson, J. Dilling, TITAN's digital RFQ ion beam cooler and buncher, operation and performance, *Nucl. Instrum. Methods Phys. Res.* ***A 676*** *(2012) 32-43.*
26. F. Herfurth, J. Dilling, A. Kellerbauer, G. Bollen, S. Henry, H.-J. Kluge, E. Lamour, D. Lunney, R.B. Moore, C. Scheidenberger, S. Schwarz, G. Sikler, J. Szerypo, A linear radiofrequency ion trap for accumulation, bunching, and emittance improvement of radioactive ion beams, Nucl. Instrum. Methods Phys. Res. **A 469** (2001) 254–275.
27. Victor Varentsov, Review of Gas Dynamic RF-only Funnel Technique for ion beams cooling and extraction into vacuum, *July 2022, DOI: 10.13140/RG.2.2.15389.18407.*
28. X.F. Yanga, S.J. Wang, S.G. Wilkins, R.F. Garcia Ruiz, Laser Spectroscopy for the Study of Exotic Nuclei, *Progress in Particle and Nuclear Physics* ***129*** **(***March 2023) 104005, https://doi.org/10.1016/j.ppnp.2022.104005.*
29. Michael Block1, Francesca Giacoppo, Fritz-Peter Heßberger, Sebastian Raeder, Recent progress in experiments on the heaviest nuclides at SHIP, *La Rivista del Nuovo Cimento* ***45*** *(2022) 279–323, https://doi.org/10.1007/s40766-022-00030-5.*
30. Piet Van Duppen, In-gas jet laser ionization spectroscopy of heavy elements, *https://www.psi.ch/sites/default/files/import/ltp/ThursdayColloquiaEN/2018_11_Laser_spectroscopy_Heavy_Elements_Piet_Van_Duppen.pdf* .
31. Yu. Kudryavtsev, R. Ferrer, M. Huyse, P. Van den Bergh, and P. Van Duppen, The in-gas-jet laser ion source: resonance ionization spectroscopy of radioactive atoms in supersonic gas jets, *Nucl. Instrum. Methods Phys. Res.* ***B 297*** *(2013) 7–22, https://doi:10.1016/j.nimb.2012.12.008.*
32. S. Raeder, M. Block, P. Chhetri, R. Ferrer, S. Kraemer, T. Kron, M. Laatiaoui, S. Nothhelfer, F. Schneider, P. Van Duppen, M. Verlinde, E. Verstraelen, Th. Walther, A. Zadvornaya, A gas-jet apparatus for high-resolution laser spectroscopy on the heaviest elements at SHIP, Nucl. Instrum. Methods Phys. Res. B **463 (**2020) 272-276, https://doi.org/10.1016/j.nimb.2019.05.016.
33. Danny Münzberg, Michael Block, Arno Claessens, Rafael Ferrer, Mustapha Laatiaoui, Jeremy Lantis, Steven Nothhelfer, Sebastian Raeder and Piet Van Duppen, Resolution Characterizations of JetRIS in Mainz Using ^{164}Dy, *Atoms 2022, 10, 57, https://doi.org/10.3390/atoms1002005.*
34. R. Ferrer, A. Barzakh, B. Bastin, R. Beerwerth, M. Block, P. Creemers, H. Grawe, R. de Groote, P. Delahaye, X. Fle´chard, S. Franchoo, S. Fritzsche, L.P. Gaffney, L. Ghys1, W. Gins, C. Granados, R. Heinke, L. Hijazi, M. Huyse, T. Kron, Yu. Kudryavtsev, M. Laatiaoui, N. Lecesne, M. Loiselet, F. Lutton, I.D. Moore, Y. Mart´ınez, E. Mogilevskiy, P. Naubereit, J. Piot, S. Raeder, S. Rothe, H. Savajols, S. Sels, V. Sonnenschein, J.-C. Thomas, E. Traykov, C. Van Beveren, P. Van den Bergh, P. Van Duppen, K. Wendt & A. Zadvornaya, Towards high-resolution laser ionization spectroscopy of the heaviest elements in supersonic gas jet expansion, *Commun.* ***8****, 14520 doi: 10.1038/ncomms14520.*

35. R. Ferrer, M. Verlinde, E. Verstraelen, A. Claessens, M. Huyse, S. Kraemer, Yu. Kudryavtsev, J. Romans, P. Van den Bergh, P. Van Duppen, and A. Zadvornaya, Hypersonic nozzle for laser-spectroscopy studies at 17 K characterized by resonance-ionization-spectroscopy-based flow mapping, *Phys. Rev. Research* ***3***, ***043041*** *(2021)* 1-18, *DOI: 10.1103/PhysRevResearch.3.043041.*
36. S. Sels, R. Ferrer, K. Dockx, C. Granados Buitrago, M. Huyse, Yu. Kudryavtsev, S. Kraemer, S. Raedera, P. Van Den Bergh, P. Van Duppen, M. Verlinde, E. Verstraelen, A. Zadvornaya, Design and commissioning of an ion guide system for In-Gas Laser Ionization and Spectroscopy experiments, *Nucl. Instrum. Methods Phys. Res.* ***B 463*** *(2020) 148-153,* https://doi.org/10.1016/j.nimb.2019.06.005.
37. Jekabs Romans, Anjali Ajayakumar, Martial Authier, Frederic Boumard, Lucia Caceres, Jean-François Cam, Arno Claessens, Samuel Damoy, Pierre Delahaye, Philippe Desrues, Antoine Drouart, Patricia Duchesne, Rafael Ferrer, Xavier Fléchard, Serge Franchoo, Patrice Gangnant, Ruben P. de Groote, Sandro Kraemer, Nathalie Lecesne, Renan Leroy, Julien Lory, Franck Lutton, Vladimir Manea, Yvan Merrer, Iain Moore, Alejandro Ortiz-Cortes, Benoit Osmond, Julien Piot, Olivier Pochon, Blaise-Maël Retailleau, Hervé Savajols, Simon Sels, Emil Traykov, Juha Uusitalo, Christophe Vandamme, Marine Vandebrouck, Paul Van den Bergh, Piet Van Duppen, Matthias Verlinde, Elise Verstraelen and Klaus Wendt, First Offline Results from the S^3 Low-Energy Branch, *Atoms 2022, 10, 21, https://doi.org/10.3390/atoms10010021.*
38. Y. Hirayama, Y. X. Watanabe, P. Schury, M. Mukai, H. Choi, M. Ahmed, Y. Kakiguchi, M. Oyaizu, M. Wada, and H. Miyatake, In-gas-jet laser ionization spectroscopy at KISS, RIKEN Accel. Prog. Rep. 52 (2019) 1.
39. V.L. Varentsov, A.A. Ignatiev, Numerical investigations of internal supersonic jet targets formation for storage rings, *Nucl. Instrum. Methods Phys. Res.* ***A 413*** *(1998) 447–456, http://dx.doi.org/10.1016/S0168-9002(98)00354-4* .
40. V.L. Varentsov, Focused ion beam source of a new type for micro- and nanoelectronic technologies*, in: Proc. SPIE,* ***7025****, (2008) 702509–702521, http://dx.doi.org/10.1117/12.802356* .
41. Victor Varentsov, Proposal of an RF-Only Double-Funnel System for Ions Extraction from a Cryogenic Stopping Cell for the Super-FRS at FAIR, GSI SCIENTIFIC *REPORT* **2015-1 (***2015) 503–504, http://dx.doi.org/10.15120/GR-2015-1-FG-SFRS-07* .
42. Victor Varentsov, Proposal of a new Laser ablation ion source for LaSpec and MATS testing, NUSTAR Collaboration Meeting *(2016), http://dx.doi.org/10.13140/RG.2.2.10904.39686.*
43. T. Brunner, D. Fudenberg, V. Varentsov, A. Sabourov, G. Gratta, J. Dilling, and nEXO Collaboration, An RF-only ion-funnel for extraction from high-pressure gases, *Int. J. Mass Spectrom.* ***379*** *(2015) 110-120, http://dx.doi.org/10.1016/j.ijms.2015.01.003*
44. Tim Ratajczyk, Philipp Bollinger, Tim Lellinger, Victor Varentsov, Wilfried Nörtershäuser, Towards a He-buffered laser ablation ion source for collinear laser spectroscopy, *Hyperfine Interact.* ***241*** *(2020) 52, http://dx.doi.org/10.1007/s10751-020-1698-0.*
45. A.A. Valverde, M. Brodeur, D.P. Burdette, J.A. Clark, J.W. Klimes, D. Lascar, P.D. O'Malley, R. Ringle, G. Savard, V. Varentsov, Stopped, bunched beams for the *twinsol* facility, *Hyperfine Interact.* ***240*** *(2019) 38, http://dx.doi.org/10.1007/s10751-019-1591-x* .
46. P.D. O'Malley, M. Brodeur, D.P. Burdette, J.W. Klimes, A. Valverde, J.A. Clark, G. Savard, R. Ringle, V. Varentsov, Testing the weak interaction using St. Benedict at the University of Notre Dame, *Nucl. Instrum. Methods Phys. Res.* ***B 463*** *(2020) 488-490, http://dx.doi.org/10.1016/j.nimb.2019.04.017.*
47. K. Murray, J. Dilling, R. Gornea, Y. Ito, T. Koffas, A.A. Kwiatkowski, Y. Lan, M.P. Reiter, V. Varentsov, T. Brunner, with the nEXO collaboration, Design of a Multiple-Reflection time-of-flight Mass-Spectrometer for Barium-tagging, *Hyperfine Interact.* ***240*** *(2019) 97, http://dx.doi.org/10.1007/s10751-019-1632-*5.
48. L. Querci, V. Varentsov, D. Günther, B. Hattendorf, An RF-only ion funnel interface for ion cooling in laser ablation time of flight mass spectrometry, *Spectrochim. Acta* ***B 146*** *(2018) 57-68, http://dx.doi.org/10.1016/j.sab.2018.05.004.*
49. D. Tiedemann, K.E. Stiebing, D.F.A. Winters, W. Quint, V. Varentsov, A. Warczak, A. Malarz, Th. Stöhlker, A pulsed supersonic gas jet target for precision spectroscopy at the HITRAP facility at GSI, *Nucl. Instrum. Methods Phys. Res.* ***A 764*** *(2014) 387–393, http://doi.org/10.1016/j.nima.2014.08.017.*
50. V.L. Varentsov, N. Kuroda, Y. Nagata, H. A. Torii, M. Shibata, and Y. Yamazaki, ASACUSA Gas-Jet Target: Present Status And Future Development, *AIP Conference Proceedings* ***793*** *(2005) 328-340, https://doi.org/10.1063/1.2121994.*
51. A. Yakushev, Y. Wey, Dimitar Simonovski, Christoph E Düllmann, Victor Vrentsov, Towards chemistry beyond moscovium (Mc, Z = 115), *Presentaion at the TASCA Collaboration Meeting, 2022, http://dx.doi.org/10.13140/RG.2.2.33574.60486*
52. V.L. Varentsov, V.V. Yaschuk, Technique of phase volume decrease of an atomic beam, in*: Inventor's Certificate (USSR) No. 774523, 1979.*

53. Varentsov V.L., Yashchuk V.V. (1983). Gasdynamic method for reducing the phase volume of an atomic beam. *Soviet Technical Physics Letters, 9(2) (1983) 65-66.*
54. V.L. Varentsov, The Method of an Atomic Beam Phase Volume Decrease and its Possible Application for Atomic and Nuclear Physics Problems (Ph.D. Thesis*), Leningrad Nuclear Physics Institute, Gatchina (1986) 1-140. In Russian.*
55. V.L. Varentsov, Gas dynamic cooling of low-energy molecular and ion beams, *J. Tech. Phys. 39 (1994) 358-363.*
56. V.L. Varentsov, V.F. Ezhov, V.A. Kniaz'kov, V.L. Ryabov, A. Yu. Khazov, V.V. Yaschuk, Time-of-flight molecular-beam spectrometer, *Prib. Tekh. Eksp. 1 (1986) 152-154.*
57. V. L. Varentsov, V. F. Ezhov, V. A. Kniaz'kov, V. G. Muratov, V. L. Ryabov, A. Yu. Khazov, V. V. Yaschuk, High-intensity gas dynamic molecular beam source of a new type, *Journal of Technical Physics, Vol. 57, No. 4 (1987) 755.*
58. V.L. Varentsov, D.R. Hansevarov, A new approach to the nozzle design of gas-jet targets, *Nucl. Instrum. Methods Phys. Res.* ***A 317*** *(1992) 1-6.*
59. V.L. Varentsov, D.R. Hansevarov, D.V. Varentsov, The generation of an internal molecular-beam target from expensive gaseous and nonvolatile substances for storage rings, *Nucl. Instrum. Methods Phys. Res. A 352 (1995) 542-547, https://doi.org/10.1016/0168-9002(95)90002-0* .
60. Victor Varentsov, Windowless gas dynamic ion beam cooler and buncher, Nucl. Instrum. Methods Phys. Res. A 984 (2020) 164596.
61. Victor Varentsov, Gas dynamic cooling of low energy molecular and ion beams, Presentation at Stefan Meyer Institute (SMI)), Vienna, April 2004, http://dx.doi.org/10.13140/RG.2.2.16530.53445